nature cell biology

# Regulation of mitochondrial biogenesis in erythropoiesis by mTORC1-mediated protein translation

Xin Liu[1,6], Yuannyu Zhang[1,2,6], Min Ni[1,6], Hui Cao[1], Robert A. J. Signer[1,3], Dan Li[1], Mushan Li[2], Zhimin Gu[1], Zeping Hu[1], Kathryn E. Dickerson[1], Samuel E. Weinberg[4], Navdeep S. Chandel[4], Ralph J. DeBerardinis[1], Feng Zhou[5,7], Zhen Shao[2,7] and Jian Xu[1,7]

**Advances in genomic profiling present new challenges of explaining how changes in DNA and RNA are translated into proteins linking genotype to phenotype. Here we compare the genome-scale proteomic and transcriptomic changes in human primary haematopoietic stem/progenitor cells and erythroid progenitors, and uncover pathways related to mitochondrial biogenesis enhanced through post-transcriptional regulation. Mitochondrial factors including TFAM and PHB2 are selectively regulated through protein translation during erythroid specification. Depletion of TFAM in erythroid cells alters intracellular metabolism, leading to elevated histone acetylation, deregulated gene expression, and defective mitochondria and erythropoiesis. Mechanistically, mTORC1 signalling is enhanced to promote translation of mitochondria-associated transcripts through TOP-like motifs. Genetic and pharmacological perturbation of mitochondria or mTORC1 specifically impairs erythropoiesis *in vitro* and *in vivo*. Our studies support a mechanism for post-transcriptional control of erythroid mitochondria and may have direct relevance to haematologic defects associated with mitochondrial diseases and ageing.**

Cellular differentiation requires highly coordinated gene expression through transcriptional and post-transcriptional mechanisms. Advances in high-throughput sequencing enabled genome-scale quantification of messenger RNA for gene expression, yet the extent to which changes in mRNA are translated to protein remains unclear. Mass spectrometry (MS)-based proteomics provide an approach to globally interrogate protein abundance in human tissues[1,2]. We reasoned that comparing the proteomic and transcriptomic profiles might provide insights into the post-transcriptional pathways in developmental specification, which would otherwise have been overlooked using only transcriptome-based analysis.

The development of haematopoietic stem/progenitor cells (HSPCs) into lineage-committed cells serves as a paradigm for studying gene regulatory events governing cellular differentiation[3]. Among them, the specification of erythroid lineage is of particular importance. An exquisite coordination of erythroid maturation is essential for continuous production of red blood cells (RBCs), and their imbalance underlies the pathogenesis of various disorders including β-thalassaemia and anaemia of chronic disease[4]. Erythroid progenitors and erythroblasts are extraordinarily proliferative, while cell growth decreases dramatically in later maturation. As haemoglobin content reaches a threshold, erythroblasts enucleate to become reticulocytes, exit the bone marrow (BM), clear the transferrin receptors, and extrude the remaining organelles including mitochondria. Little is known about how differentiating erythroid cells coordinate programs of proliferation, maturation and metabolism with the changing environment and cellular processes.

Through an unbiased analysis of proteomic and transcriptomic changes during human erythropoiesis, we uncovered major pathways related to mitochondrial biogenesis enhanced through post-transcriptional pathways. In-depth molecular and genetic studies established a functional link between mitochondrial metabolism and epigenetic regulation required for normal erythropoiesis. Our results support a model in which the erythroid mitochondria

[1]Children's Medical Center Research Institute, Department of Pediatrics, University of Texas Southwestern Medical Center, Dallas, Texas 75390, USA. [2]Key Laboratory of Computational Biology, Collaborative Innovation Center for Genetics and Developmental Biology, CAS-MPG Partner Institute for Computational Biology, Shanghai Institutes for Biological Sciences, Chinese Academy of Sciences, Shanghai 200031, China. [3]Division of Regenerative Medicine, Department of Medicine, Moores Cancer Center, University of California San Diego, La Jolla, California 92093, USA. [4]Department of Medicine, Northwestern University Feinberg School of Medicine, Chicago, Illinois 60611, USA. [5]Liver Cancer Institute, Zhongshan Hospital, Key Laboratory of Carcinogenesis and Cancer Invasion, Minister of Education, and Institutes of Biomedical Sciences, Fudan University, Shanghai 200032, China. [6]These authors contributed equally to this work.
[7]Correspondence should be addressed to F.Z., Z.S. or J.X. (e-mail: zhou_feng@fudan.edu.cn or shaozhen@picb.ac.cn or jian.xu@utsouthwestern.edu)

Received 14 October 2016; accepted 6 April 2017; published online 15 May 2017; DOI: 10.1038/ncb3527

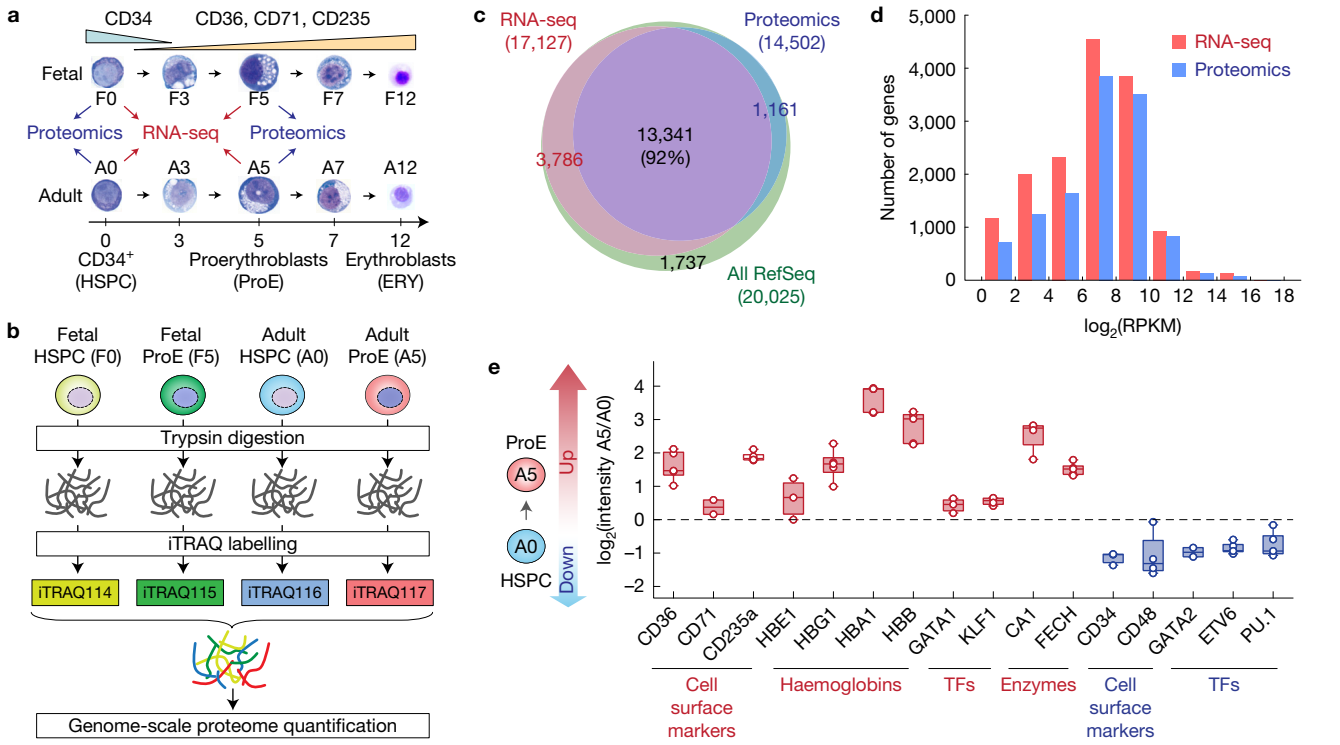


**Figure 1** Comparative proteomic and transcriptomic analyses of human erythropoiesis. (**a**) Fetal and adult-stage CD34$^+$ HSPCs were differentiated into ProEs *ex vivo*. Cells at matched stages of differentiation were collected for RNA-seq ($n=4$ independent experiments) and proteomic ($n=5$ independent experiments) analyses. (**b**) Schematic of iTRAQ-based quantitative proteomic analysis. (**c**) Venn diagram shows overlap between identified mRNA transcripts and proteins. (**d**) Overlay of RNA-seq and proteomic data demonstrates that the proteomic analysis achieved a comparable range of quantification as the RNA-seq-based transcriptomic profiling. RPKM, reads per kilobase of transcript per million reads. $n=4$ independent RNA-seq experiments and $n=5$ independent proteomic experiments. (**e**) Changes in expression of representative proteins between adult-stage HSPCs (A0) and ProEs (A5) are shown. Each coloured circle represents the measurement from an independent experiment. Boxes show the mean of the data and quartiles ($n=4$ independent RNA-seq experiments and $n=5$ independent proteomic experiments). Whiskers show the minimum and maximum of the data.

are regulated by mTORC1-mediated protein translation and may have direct relevance to haematologic disorders associated with mitochondrial dysregulation.

## RESULTS

### Comparative proteomic and transcriptomic profiling of erythropoiesis

Human CD34$^+$ HSPCs were differentiated *ex vivo* into erythroid progenitors (proerythroblasts or ProEs) and late erythroblasts (ERYs)[5] (Fig. 1a). Fetal or adult HSPCs (F0 or A0) and lineage-committed ProEs (F5 or A5) were selected for genome-scale quantification of proteins and mRNAs by MS-based proteomics and RNA-seq analysis, respectively (Fig. 1b). Proteomic profiling using multiplexed isobaric tags (iTRAQ) resulted in identification and quantification of proteins encoded by 14,502 genes, accounting for 72.4% of annotated protein-coding genes[6] (Supplementary Table 1). Among them, 92.0% (13,341 of 14,502) were assigned to corresponding transcripts detected by RNA-seq (Fig. 1c). The proteomic and transcriptomic profiling achieved comparable ranges of quantification (Fig. 1d). A survey of representative genes demonstrated reproducible increases in expression of erythroid-associated markers (CD36, CD71 and CD235a), haemoglobins (HBE1, HBG1, HBB and HBA1), transcription factors (TFs) (GATA1 and KLF1) and enzymes (CA1 and FECH) in ProEs relative to HSPCs. Similarly, the expression of HSPC-associated markers and TFs was significantly decreased in ProEs (Fig. 1e). In total, we identified 1,071 to 2,598 differentially expressed mRNAs (fold change $\geq 1.5$, $P$ value $\leq 0.01$; Supplementary Fig. 1a–h and Supplementary Table 2) and 393 to 1,663 differentially expressed proteins (fold change $\geq 1.3$, $P$ value $\leq 0.01$; Supplementary Fig. 1i–p and Supplementary Table 3) associated with distinct biological processes between fetal or adult HSPCs and ProEs, respectively.

### Post-transcriptional control of proteins associated with mitochondrial biogenesis

To compare mRNA and protein-level expression, we overlaid the transcriptomic and proteomic profiles between adult HSPCs (A0) and ProEs (A5) (Fig. 2a). Strikingly, 1,050 out of 1,549 (67.8%) upregulated proteins were not paralleled by changes in cognate mRNAs. Similarly, 399 out of 785 (50.8%) downregulated proteins had no corresponding change in mRNAs. Similar patterns were observed between fetal HSPCs and ProEs (Supplementary Fig. 1r–t). We also identified differentially expressed mRNAs with no changes in proteins, consistent with regulation through mRNA stability, translation and/or protein stability.

Hereafter we focused on adult HSPCs and ProEs. We categorized the upregulated genes into three groups (RNA-only, Both and

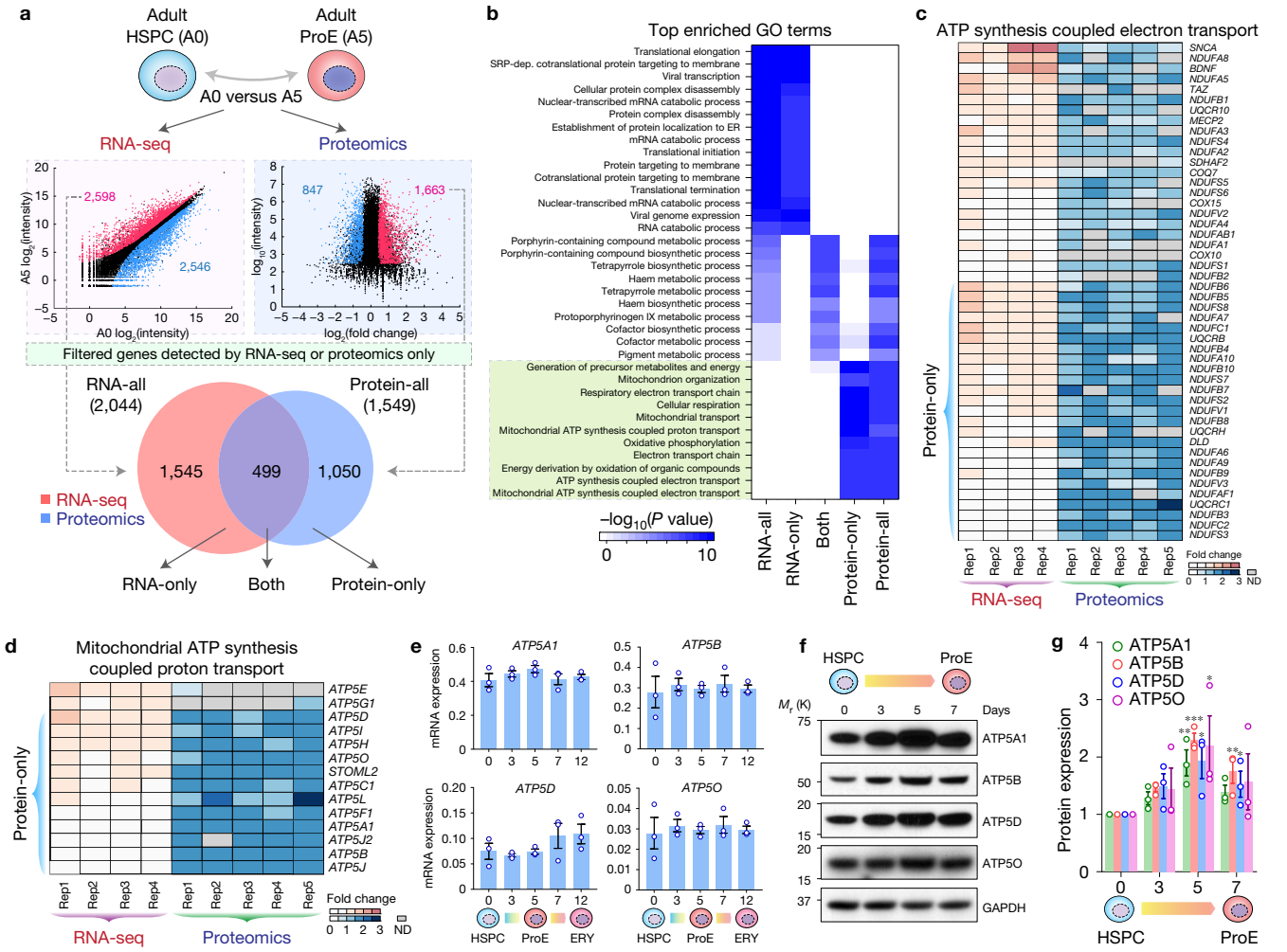


**Figure 2** Comparative transcriptomic and proteomic analyses revealed post-transcriptional control of mitochondrial pathways. (**a**) The correlation between RNA and protein-level expression changes in adult-stage HSPCs (A0) and ProEs (A5). Differentially expressed RNA transcripts and proteins (red, upregulated; blue, downregulated) were accessed for overlap. After filtering genes detected exclusively by RNA-seq or proteomics, 2,044 and 1,549 significantly upregulated RNAs (RNA-all) and proteins (Protein-all) were identified, respectively. The differentially expressed genes were further divided into three groups based on significant changes at RNA (RNA-only), protein (Protein-only), and both levels, respectively. (**b**) GO enrichment analysis of protein and RNA expression changes. The green box highlights the top enriched GO terms for Protein-only genes. (**c**) Expression heatmap for genes associated with 'ATP synthesis coupled electron transport'. The Protein-only genes are shown on the bottom. ND, not detected. (**d**) Expression heatmap for genes associated with 'Mitochondria ATP synthesis coupled proton transport'. (**e**) mRNA expression of representative Protein-only genes (*ATP5A1*, *ATP5B*, *ATP5D* and *ATP5O*) was measured by qRT–PCR in HSPCs and differentiating erythroid cells. Results are mean ± s.e.m. ($n=3$ independent experiments). (**f**) Western blot analysis of representative Protein-only genes. (**g**) Quantification of western blot analysis. Results are mean ± s.e.m. ($n=3$ independent experiments). Differences relative to HSPCs (day 0) were assessed using a repeated-measures one-way ANOVA followed by Dunnett's test for multiple comparisons. $^{*}P<0.05$, $^{**}P<0.01$, $^{***}P<0.001$ relative to HSPCs (day 0) were considered significant. See Statistics Source Data in Supplementary Table 8. Unprocessed original scans of blots are shown in Supplementary Fig. 9.

Protein-only; Fig. 2a; Supplementary Table 4) based on the changes in mRNA and protein expression. By gene ontology (GO), the 'Both' genes are highly associated with haem biosynthetic processes that are hallmarks of erythroid differentiation. Strikingly, the most enriched pathways in 'Protein-only' genes are related to mitochondrial biogenesis, including ATP biosynthesis, electron transport chain and oxidative phosphorylation (Fig. 2b and Supplementary Fig. 2a–e). Known mitochondrial genes[7,8] are enriched most significantly in the upregulated 'Protein-only' genes (Supplementary Fig. 2f,g).

Notably, 25 of 48 proteins related to 'ATP synthesis coupled electron transport' were significantly upregulated with little or no changes in mRNAs in ProEs (Fig. 2c). Similarly, 12 of 14 proteins related to 'mitochondrial ATP synthesis coupled proton transport' were markedly upregulated without changes in mRNAs (Fig. 2d). These findings were validated by quantitative PCR with reverse transcription (qRT–PCR) and western blot analyses of major components of the mitochondrial $H^{+}$-ATP synthases ATP5A1, ATP5B, ATP5D and ATP5O (Fig. 2e–g). Our results suggest that the expression of mitochondrial proteins is enhanced through post-transcriptional mechanisms during erythropoiesis.

## Mitochondria are highly regulated during erythroid differentiation

Mitochondria are critical for haem and iron metabolism, yet their regulation during erythropoiesis remains elusive. We measured

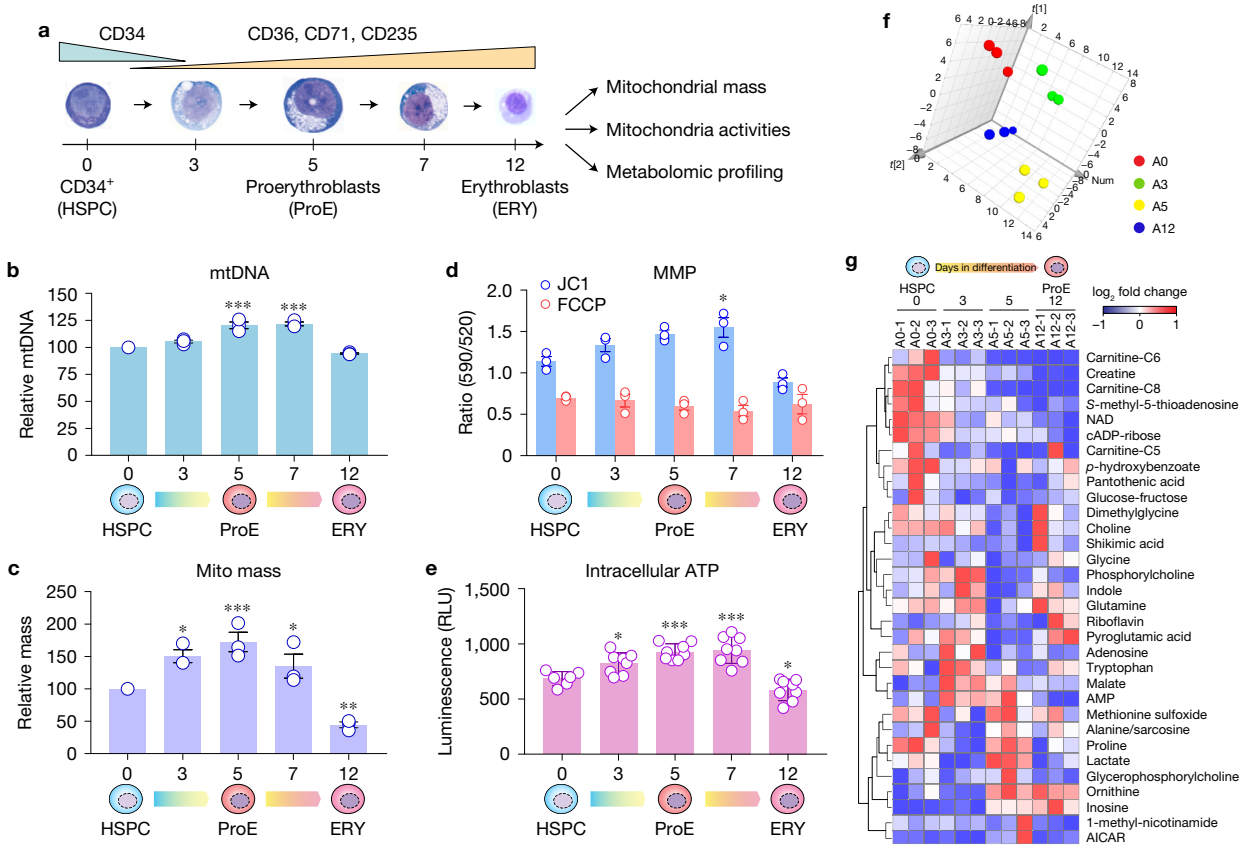


**Figure 3** Dynamic regulation of mitochondria during erythroid differentiation. (**a**) Analysis of mitochondrial biogenesis and activities during human erythropoiesis. (**b**) Mitochondrial DNA (mtDNA) was determined using qPCR-based analysis to measure the ratio of mitochondrial DNA (ND1) versus genomic DNA (18S). The mtDNA content at various stages of erythroid differentiation relative to undifferentiated HSPC (day 0) is shown. (**c**) Mitochondrial mass was determined by flow cytometry using MitoTracker Green. The mitochondrial mass relative to undifferentiated HSPC (day 0) is shown. (**d**) Changes in mitochondrial membrane potential (MMP) was monitored by staining with JC1. Cells treated with the protonophore FCCP were analysed as controls. All data are mean ± s.e.m. ($n=3$ independent experiments) (**b**–**d**). (**e**) Changes in intracellular ATP during erythroid differentiation. RLU, relative light unit. Results are mean ± s.d. of $n=6$ (day 0) or $n=8$ (day 3 to day 12) independent measurements pooled from 4 experiments. Differences relative to HSPCs (day 0) were assessed using a repeated-measures one-way ANOVA followed by Dunnett's test for multiple comparisons (**b**–**e**). $^{*}P<0.05$, $^{**}P<0.01$, $^{***}P<0.001$ relative to HSPCs were considered significant. (**f**) Principle component analysis of metabolomic profiles in adult HSPCs (A0) and differentiating erythroid cells (A3, A5 and A12). $n=3$ biological replicate samples for each group. (**g**) Heatmap for metabolites with significant changes (see Methods) during erythropoiesis. Unsupervised clustering of metabolites according to the changes in their amounts during differentiation is shown. See Statistics Source Data in Supplementary Table 8.

mitochondrial mass and activities in CD34$^{+}$ HSPCs, ProEs and late erythroblasts (Fig. 3a). Consistent with enhanced expression of mitochondrial proteins, we observed progressive increases in mitochondrial DNA (mtDNA), mitochondrial mass, membrane potential (MMP) and intracellular ATP during erythroid specification (days 3 to 7) before clearance of mitochondria following terminal maturation (Fig. 3b–e). By profiling metabolites involved in major bioenergetic pathways, we observed progressive alterations of the central carbon and other metabolic pathways, such as purine and amino acid metabolism, during erythropoiesis (Fig. 3f,g). Moreover, mtDNA was significantly elevated during erythropoiesis in mouse fetal liver (FL) and BM (R2 and R3 stages[9]; Supplementary Fig. 3).

## TFAM and PHB2 are post-transcriptionally regulated during erythropoiesis

We next surveyed annotated human TFs (refs 10,11) and identified 28 TFs whose proteins but not mRNAs were significantly increased during erythropoiesis (Fig. 4a). Notably, Prohibitin 2 (PHB2) and mitochondrial transcription factor A (TFAM) were ranked second and third on the basis of the significance of increased protein expression (Fig. 4a). TFAM is essential for transcription and replication of mitochondrial genome[12,13], while PHB2 plays a critical scaffolding role on mitochondrial inner membrane. The expression of TFAM or PHB2 proteins and mRNAs was validated by qRT–PCR and western blot (Fig. 4b–d). TFAM and PHB2 proteins were also increased in mouse FL and BM erythropoiesis (Supplementary Fig. 3). Furthermore, the half-lives of TFAM and PHB2 proteins, as determined by cycloheximide (CHX) chase experiments, were comparable between HSPCs and ProEs, suggesting that the elevated protein expression is not due to increased protein stability (Fig. 4e,f).

## TFAM and PHB2 are indispensable for mitochondria and erythropoiesis

To determine the role of TFAM and PHB2, we employed short hairpin RNA (shRNA)-mediated depletion (Fig. 4g). TFAM- or

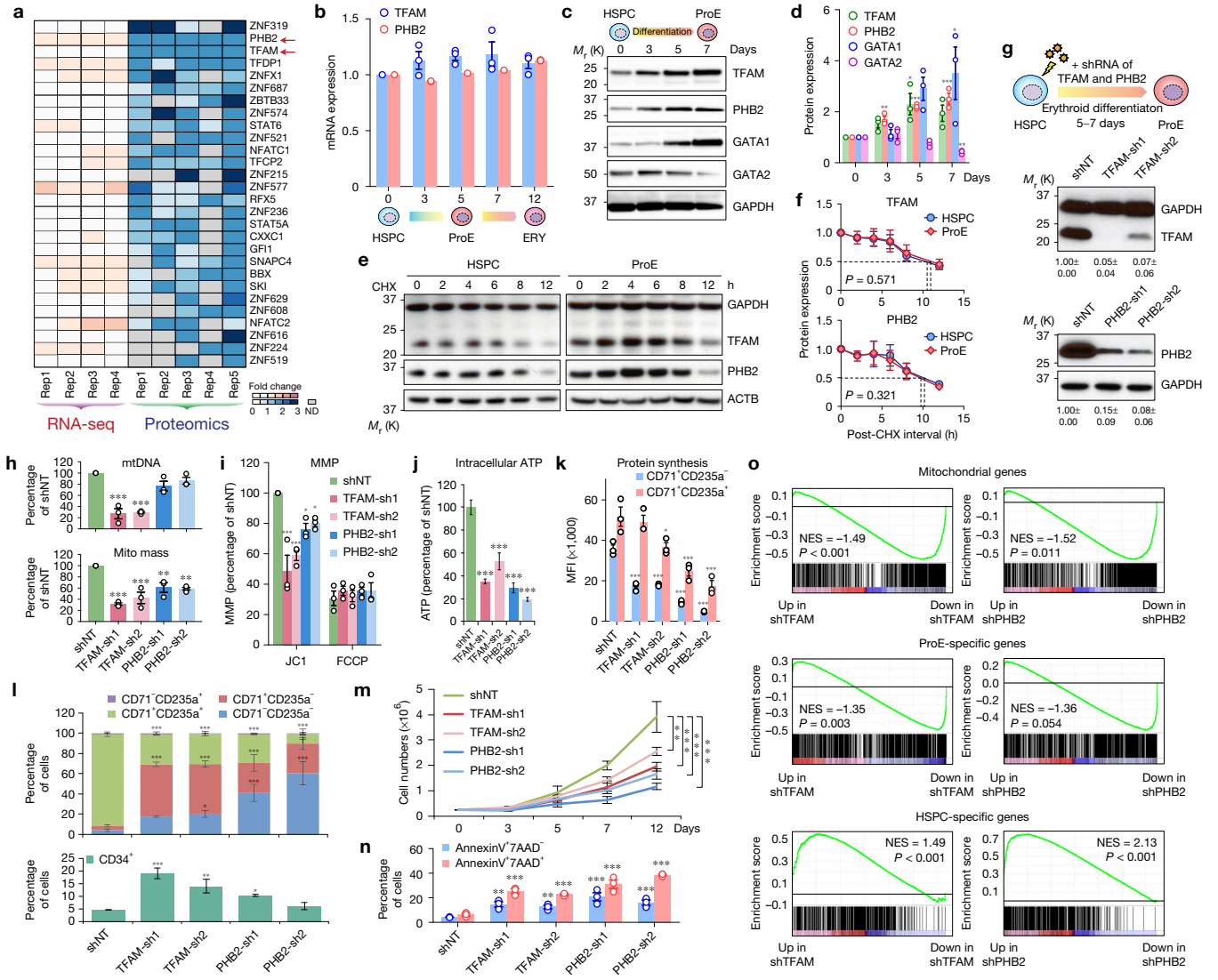


**Figure 4** TFAM and PHB2 are post-transcriptionally regulated and indispensable for mitochondria and erythropoiesis. (**a**) Heatmap for transcription factors significantly upregulated at the protein but not mRNA levels. The genes are ranked on the basis of the significance of fold changes in protein expression between HSPCs (A0) and ProEs (A5). ND, not detected. (**b**) qRT–PCR analysis of *TFAM* and *PHB2* in HSPCs and differentiating erythroid cells. (**c**) Western blot of TFAM, PHB2, GATA1 and GATA2 in HSPCs and erythroid cells. (**d**) Quantification of western blot analysis. (**e**) The protein half-lives of TFAM and PHB2 were determined by CHX chase experiments. (**f**) Quantification of TFAM and PHB2 half-lives in HSPCs and ProEs. The dashed lines indicate the calculated half-lives for both proteins. Results are mean ± s.e.m. of $n=3$ independent experiments (**b**,**d**,**f**). Differences relative to HSPCs (day 0) were assessed using a repeated-measures one-way ANOVA followed by Dunnett's test for multiple comparisons. $^{*}P<0.05$, $^{**}P<0.01$, $^{***}P<0.001$ (**b**,**d**,**f**). (**g**) Schematic of lentiviral shRNA-mediated depletion of TFAM or PHB2 in HSPCs, followed by erythroid differentiation (top). Validation of TFAM or PHB2 depletion by western blot (bottom). Cells transduced with non-targeting shRNA (shNT) were analysed as controls. The quantified protein expression of TFAM or PHB2 from three independent experiments is shown as mean ± s.e.m. on the bottom. (**h**) Depletion of TFAM significantly decreased mtDNA (top). TFAM and PHB2 depletion significantly decreased mitochondrial mass (bottom). (**i**–**n**) Depletion of TFAM or PHB2 significantly decreased MMP (**i**), intracellular ATP (**j**), protein synthesis in CD71$^{+}$CD235a$^{-}$ and CD71$^{+}$CD235a$^{+}$ erythroid progenitors (**k**), erythroid differentiation measured by the expression of CD34, CD71 and CD235a (**l**), proliferation (**m**), and increased apoptosis by AnnexinV and 7-AAD staining (**n**). MFI, mean fluorescence intensity. Results are mean ± s.e.m. of $n=3$ independent experiments (**h**,**i**,**k**–**n**) or mean ± s.d. of $n=8$ independent measurements from three experiments (**j**). Differences relative to shNT were assessed using a repeated-measures one-way ANOVA followed by Dunnett's test for multiple comparisons; $^{*}P<0.05$, $^{**}P<0.01$, $^{***}P<0.001$ (**h**–**n**). (**o**) GSEA analysis of mitochondrial genes, ProE- or HSPC-specific genes using the RNA-seq of shTFAM or shPHB2 relative to shNT, respectively. NES, normalized enrichment score. See Statistics Source Data in Supplementary Table 8. Unprocessed original scans of blots are shown in Supplementary Fig. 9.

PHB2-deficient ProEs displayed significant decreases in mtDNA, mitochondrial mass, MMP and ATP compared with control cells expressing the non-targeting shRNA (shNT) (Fig. 4h–j). By measuring the incorporation of the methionine analogue L-homopropargylglycine (HPG)[14], we observed a markedly reduced rate of protein synthesis in TFAM- or PHB2-depleted early (CD71$^{+}$CD235a$^{-}$) and late (CD71$^{+}$CD235a$^{+}$) erythroid progenitors (Fig. 4k). TFAM or PHB2 depletion impaired erythroid differentiation, proliferation and increased apoptosis (Fig. 4l–n). TFAM- or PHB2-depleted cells appeared morphologically immature with

decreased expression of haemoglobins and *GATA1* (Supplementary Fig. 4a–c). We then performed RNA-seq analysis of control, TFAM- and PHB2-depleted CD71$^+$CD235a$^+$ cells. By gene-set enrichment analysis (GSEA)[15], we observed that the mitochondrial[8] and ProE-specific genes (Supplementary Table 2) were significantly downregulated whereas HSPC-specific genes (Supplementary Table 2) were upregulated in TFAM or PHB2-depleted cells (Fig. 4o; Supplementary Table 5). These findings demonstrate that TFAM or PHB2 loss impaired the silencing of HSPC genes and the expression of genes required for mitochondria and erythropoiesis.

### TFAM is indispensable for erythropoiesis *in vivo*

To establish the *in vivo* function, we generated the erythroid-specific *Tfam* knockout (KO) mice by EpoR-Cre[16]. We found that the embryonic day (E)13.5 *EpoR-Cre*$^+$*;Tfam*$^{fl/fl}$ embryos (hereafter called *Tfam* KO) were pale and anaemic compared with littermates (Fig. 5a). Tfam protein was absent in CD71$^+$Ter119$^+$ KO erythroid cells and reduced in *EpoR-Cre*$^+$*;Tfam*$^{fl/+}$ (heterozygous KO or HET) erythroid cells (Fig. 5b). Consistent with the reduced size (Fig. 5a), the cellularity of *Tfam* KO fetal livers is 45% of the wild-type (WT) controls (Fig. 5c). Erythroid maturation can be analysed by the expression of CD71 and Ter119 markers (R1 to R5) (ref. 9) (Fig. 5d). *Tfam* KO led to substantial increases in R1 and R2 cells and a marked decrease in R3 erythroid progenitors (Fig. 5e,f). *Tfam* HET mice displayed intermediate phenotypes. *Tfam* KO also led to decreased mitochondrial mass and significantly increased apoptosis (Fig. 5g,h and Supplementary Fig. 5).

We then performed RNA-seq of *Tfam* WT and KO CD71$^+$Ter119$^+$ E13.5 erythroid cells. We identified 106 significantly upregulated and 249 downregulated genes in *Tfam* KO (Supplementary Table 6). The downregulated genes are highly associated with mitochondrial metabolism (Fig. 5i,j). The mitochondrial signature genes[8] and genes associated with reactive oxygen species, oxidative phosphorylation, arginine and proline metabolism were markedly downregulated in *Tfam* KO (Fig. 5k). Together these analyses provide compelling evidence that Tfam is indispensable for proper control of metabolism and gene expression during erythropoiesis *in vivo*.

### TFAM loss leads to altered metabolism and histone hyperacetylation

Changes in metabolism often result in altered epigenetic regulation[17]. We then measured histone modifications and observed significant increases in the levels of acetylated histones in TFAM-deficient erythroid cells (Fig. 6a and Supplementary Fig. 6a–d). Acetylated histones including H3K27ac are associated with gene activation. By ChIP-seq, we observed that TFAM depletion led to markedly increased H3K27ac at the promoters of the HSPC-specific genes (Fig. 6b,c and Supplementary Fig. 6e), consistent with the increased expression of HSPC genes. In total, 1,214 ChIP-seq peaks showed upregulated H3K27ac in TFAM-deficient erythroid cells (Fig. 6d). The upregulated peaks were highly associated with lymphoid development and haematopoiesis (Fig. 6e), suggesting that histone hyperacetylation results in altered epigenetic regulation.

To establish the causality, we performed metabolomic analysis and identified 32 and 39 significantly upregulated and downregulated metabolites in TFAM-depleted erythroid cells (Fig. 6f,g and Supplementary Fig. 6f,g). Notably, β-hydroxybutyrate (βOHB) was among the most upregulated metabolites. The ketone body βOHB is synthesized from acetyl-CoA by β-hydroxybutyrate dehydrogenase as an alternative energy source[18]. Importantly, βOHB and the related butyrate are potent inhibitors of class I and II histone deacetylases (HDACs)[18]. Thus, our results suggest that the increased histone acetylation may be due to HDAC inhibition. Consistently, TFAM depletion led to significantly decreased HDAC activities (Fig. 6h). The level of acetyl-CoA was also lower (Fig. 6i), suggesting that the increased histone acetylation was not due to enhanced histone acetyltransferase activity[19]. Furthermore, human erythroid cells treated with βOHB or butyrate markedly enhanced histone acetylation, increased expression of the HSPC gene *GATA2* and impaired erythroid differentiation in a dose-dependent manner (Fig. 6j–l).

Together our results suggest that loss of TFAM causes defective mitochondria and metabolism, resulting in increased βOHB and HDAC inhibition. Increased histone acetylation interferes with the developmental silencing of HSPC genes, resulting in impaired erythroid gene expression and differentiation. Hence, our findings provide a molecular link between mitochondrial biogenesis, metabolism and epigenetic regulation required for normal erythropoiesis (Fig. 6m).

### Translation of mitochondria-related mRNAs is enhanced during erythropoiesis

Increased translation provides an efficient way to control protein production in stem cells[14] and cancer[20,21]. We hypothesized that mitochondria-associated mRNAs are regulated through enhanced protein translation during erythropoiesis. Consistently, the rate of protein synthesis was the lowest in CD34$^+$ HSPCs and increased by 2.1-fold in differentiated CD34$^-$ populations (Fig. 7a). Importantly, protein synthesis was increased by 1.8- and 2.5-fold in early (CD71$^+$CD235a$^-$) and late (CD71$^+$CD235a$^+$) erythroid progenitors, suggesting that erythroid differentiation from HSPCs is accompanied by enhanced protein translation. Furthermore, we performed polysome profiling and observed increased polysome size, indicating enhanced protein translation in ProEs relative to HSPCs (Fig. 7b). By qRT–PCR analysis of the polysomal fractions, we observed enhanced translation of mitochondria-related mRNAs in ProEs, as illustrated by a shift of these mRNAs towards larger polysomes (Fig. 7c). The translation of *GATA1* but not *ACTB* was also increased, suggesting that erythroid differentiation is accompanied by enhanced translation of a subset of, but not all, mRNAs.

### Enhanced mTORC1 signalling regulates mitochondrial biogenesis during erythropoiesis

The serine/threonine kinase mTOR is a major regulator of protein translation[22]. Genetic or pharmacologic perturbation of mTORC1, but not mTORC2, impaired erythroid development in mouse[23,24]. Activated mTORC1 phosphorylates 4EBP1 and S6K to promote protein translation[25]. Consistently, we observed a gradual increase of mTORC1 signalling, as measured by the levels of phosphorylated 4EBP1 and S6K, and mitochondrial proteins during erythroid differentiation (Fig. 7d). Moreover, HSPCs treated with rapamycin or the active-site mTOR inhibitors (asTORi) PP242 (ref. 26) and Torin1 (ref. 27) decreased 4EBP1 phosphorylation and mitochondrial

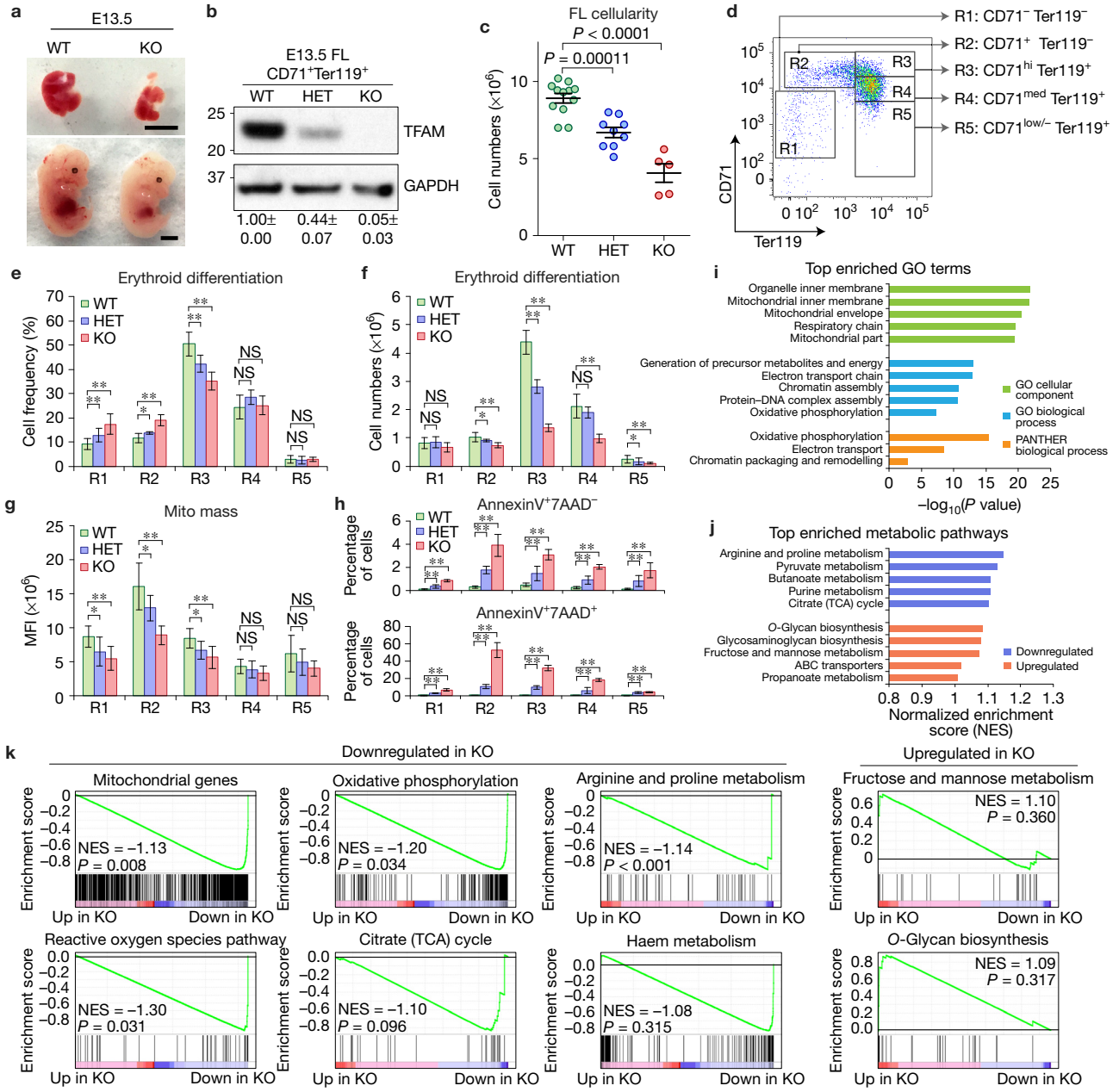


**Figure 5** TFAM and PHB2 are required for erythroid development *in vivo*. (**a**) Representative pictures of E13.5 *Tfam* WT and KO embryos (bottom) and fetal livers (top). Scale bars, 0.5 cm. (**b**) Western blot of TFAM expression in WT, HET and KO CD71$^+$Ter119$^+$ E13.5 fetal liver erythroid cells. The quantified protein expression of TFAM is shown on the bottom as mean ± s.e.m. of four independent samples for each genotype. (**c**) Total cell numbers in control (WT; $n=12$), *Tfam* HET ($n=9$) and KO ($n=5$) E13.5 fetal livers. (**d**) Erythroid differentiation was assessed by expression of CD71 and Ter119. (**e**,**f**) The frequency and number of R1 to R5 cells in *Tfam* WT ($n=16$), HET ($n=6$) and KO ($n=4$) E13.5 fetal livers. (**g**) Mitochondrial mass was determined by MitoTracker Green in *Tfam* WT ($n=16$), HET ($n=6$) and KO ($n=4$) E13.5 erythroid cells. (**h**) Cell apoptosis in *Tfam* WT ($n=6$), HET ($n=5$) and KO ($n=4$) E13.5 erythroid cells. Results are mean ± s.d. (**c**,**e**–**h**) and analysed by one-way ANOVA (**c**) or a two-tailed *t*-test (**e**–**h**) to evaluate the differences between WT and KO (or HET). $^*P<0.05$, $^{**}P<0.01$ were considered significant. NS, not significant. (**i**) Top enriched GO terms in significantly downregulated genes in *Tfam* KO erythroid cells. (**j**) Top enriched metabolic pathways in downregulated or upregulated genes in *Tfam* KO erythroid cells. (**k**) GSEA analysis of mitochondrial genes and other indicated signature genes downregulated or upregulated in *Tfam* KO erythroid cells. See Statistics Source Data in Supplementary Table 8. Unprocessed original scans of blots are shown in Supplementary Fig. 9.

proteins, mtDNA, MMP, ATP, protein synthesis, and impaired erythroid differentiation (Fig. 7e–k and Supplementary Fig. 7d–f).

To assess the *in vivo* effects, we treated adult mice with PP242 and Torin1 (Fig. 7l). Acute mTORC1 inhibition had profound effects on 4EBP1 phosphorylation, TFAM and PHB2 expression in CD71$^+$Ter119$^+$ erythroid cells (Fig. 7l), and decreased RBCs (Fig. 7m). While the BM cellularity remained unchanged, the frequencies of immature (CD71$^+$Ter119$^+$) and mature (CD71$^-$Ter119$^+$) erythroid cells were significantly lower in asTORi-treated mice (Fig. 7n). mTORC1 inhibition led to significantly increased R1/R2

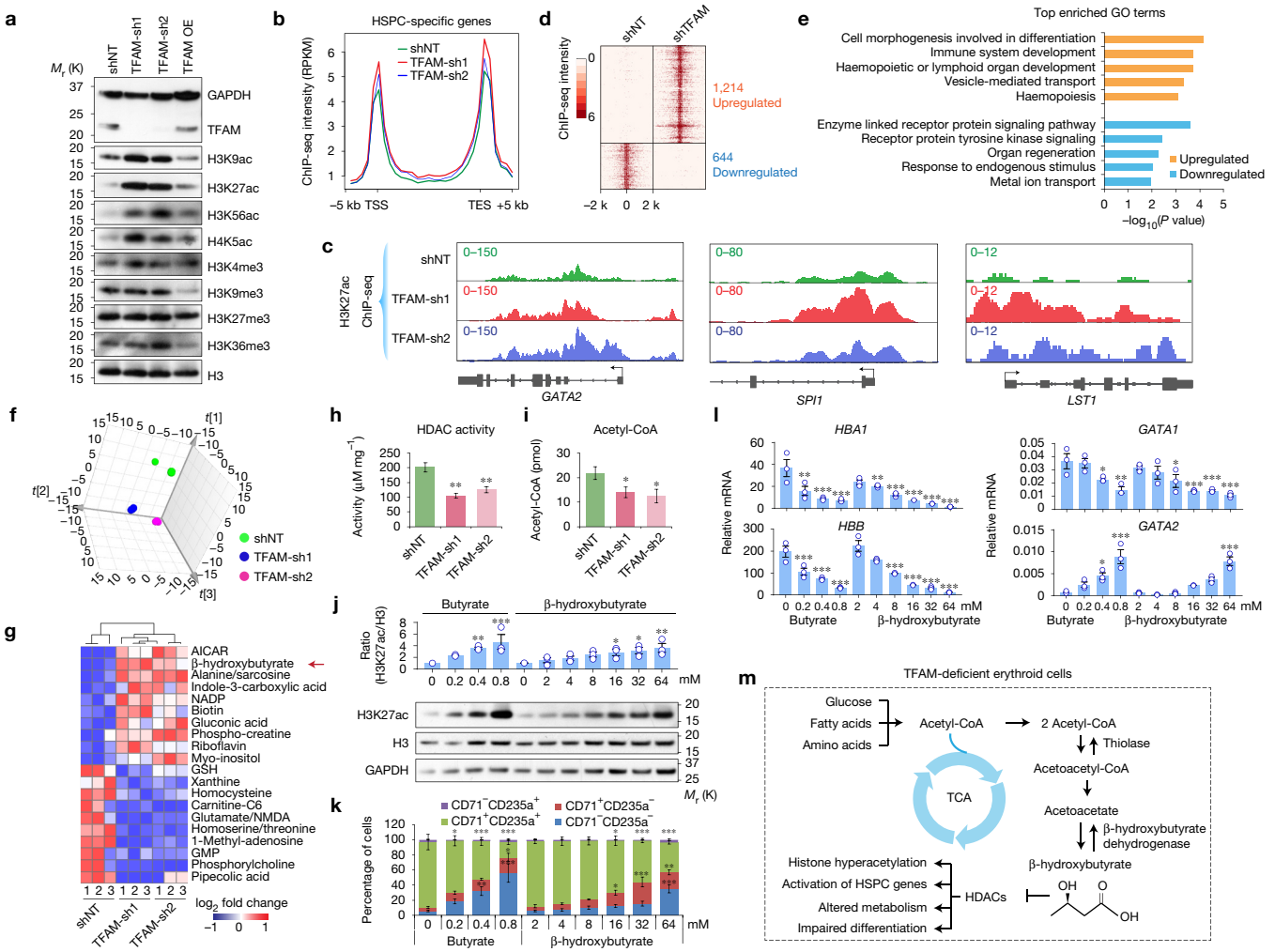


**Figure 6** TFAM depletion leads to altered metabolism and histone hyperacetylation in erythroid cells. (**a**) Western blot of histone modifications in human erythroid (K562) cells transduced with TFAM shRNAs, control (shNT), or overexpression (OE) constructs. Quantification of western blot is shown in Supplementary Fig. 6a. (**b**) The distribution of H3K27ac intensity at HSPC-specific genes. The average ChIP-seq intensity (RPKM) is shown between 5 kb upstream of the transcription start site (TSS) and downstream of the transcription end site (TES). (**c**) H3K27ac ChIP-seq density plots for three representative HSPC-specific genes. (**d**) Heatmap for differentially enriched H3K27ac ChIP-seq peaks. 1,214 upregulated and 644 downregulated H3K27ac peaks were identified with >4-fold changes in intensity between shTFAM and shNT. (**e**) Top enriched GO terms in genes associated with the upregulated or downregulated H3K27ac peaks. (**f**) Principle component analysis of metabolomic profiles in K562 erythroid cells transduced with control or TFAM shRNAs. $n=3$ biological replicates per group. (**g**) Heatmap of the top 10 most upregulated or downregulated metabolites between control and TFAM-depleted erythroid cells. (**h**) HDAC activity in erythroid cells transduced with TFAM or control shRNAs. (**i**) Acetyl-CoA level in erythroid cells transduced with TFAM or control shRNAs. Results are mean ± s.e.m. of $n=7$ (**h**) or $n=5$ (**i**) independent measurements. Differences relative to shNT were analysed by a two-tailed *t*-test. $^{*}P<0.05$, $^{**}P<0.01$. (**j**) Western blot of H3K27ac and H3 in human primary erythroid cells treated with butyrate or β-hydroxybutyrate for 12 h. Quantification of western blot is shown on the top. Results are mean ± s.e.m. of $n=3$ experiments. (**k**) Erythroid differentiation was assessed by CD71 and CD235a. Results are mean ± s.e.m. of $n=3$ experiments. (**l**) mRNA expression of haemoglobin genes (*HBA1* and *HBB*), *GATA1* and *GATA2*. Results are mean ± s.e.m. of $n=3$ experiments. Differences relative to control cells (0 mM) were assessed using a repeated-measures one-way ANOVA with Dunnett's test for multiple comparisons; $^{*}P<0.05$, $^{**}P<0.01$, $^{***}P<0.001$ (**j**–**l**). (**m**) Schematic of changes in metabolism and histone acetylation in TFAM-deficient erythroid cells. See Statistics Source Data in Supplementary Table 8. Unprocessed original scans of blots are shown in Supplementary Fig. 9.

progenitors and decreased R3/R4 erythroid cells, similar to *Tfam* KO (Fig. 7o) and mice harbouring deletion of the mTOR kinase[28]. Furthermore, mTORC1 inhibition significantly decreased mitochondrial mass and MMP in R2 and R3 cells (Fig. 7p,q), indicating that the erythroid commitment from R2 to R3 stages is selectively sensitive to mTORC1 inhibition.

We next determined the effects of mTORC1 hyperactivation by depleting TSC1 and TSC2, the negative regulators of mTORC1 (ref. 29). TSC1 or TSC2 depletion in erythroid cells significantly increased mtDNA, mitochondrial mass and MMP (Fig. 7r and Supplementary Fig. 7g–i). mTORC1 hyperactivation also impaired erythroid differentiation and increased apoptosis (Supplementary Fig. 7j,k) consistent with previous studies[23], suggesting that the coordinated control of mTORC1 and mitochondria is essential for erythropoiesis. Similarly, haematopoietic-specific KO of *Pten*, a negative regulator of AKT and mTORC1 (ref. 30), significantly augmented

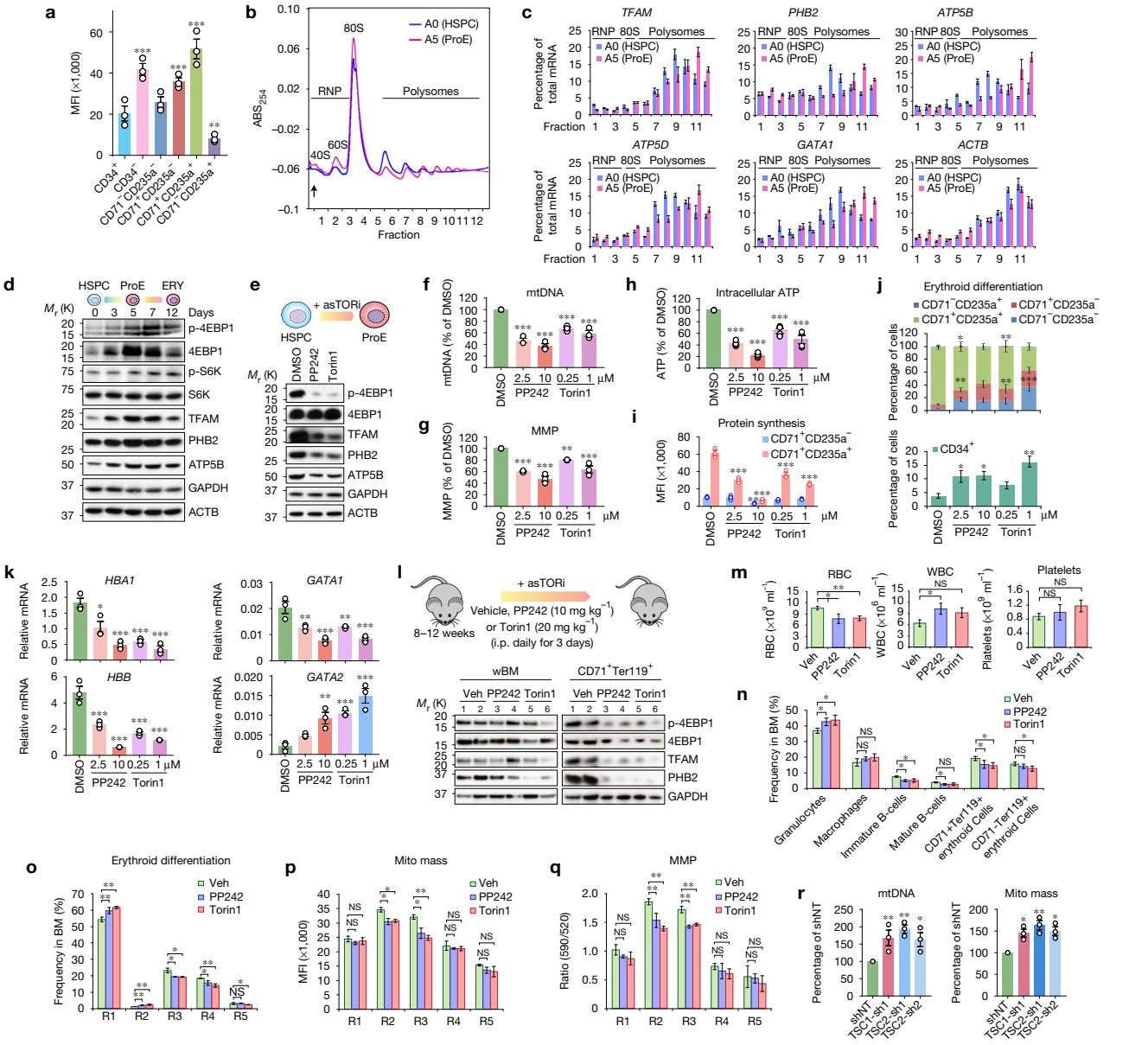


**Figure 7** mTORC1 regulates mitochondrial biogenesis in erythroid cells. (**a**) Protein synthesis was assessed by HPG incorporation. Results are mean ± s.e.m. of $n=3$ experiments. Differences relative to $CD34^+$ were assessed using a repeated-measures one-way ANOVA with Dunnett's test for multiple comparisons. $^{**}P<0.01$, $^{***}P<0.001$. (**b**) Polysome profiling of HSPCs and ProEs. A representative profile is shown where the arrow represents the start of fraction. The positions of ribonucleoproteins (RNP), 80S ribosomes and polysomes are indicated. $ABS_{254}$, absorbance at 254 nm. (**c**) qRT–PCR analysis of polysome fractions in HSPCs and ProEs. Results are mean ± s.d. of $n=4$ measurements and shown as the percentage (%) of total mRNA of all fractions combined. (**d**) Western blot analysis in HSPCs and erythroid cells. (**e**) HSPCs treated with control (DMSO), PP242 (2.5 μM) or Torin1 (0.25 μM) during erythroid differentiation for 5–7 days were analysed by western blot. (**f**–**k**) mTORC1 inhibition decreased mtDNA (**f**), MMP (**g**), ATP (**h**), protein synthesis (**i**), and impaired erythroid maturation (**j**) and gene expression (**k**). Results are mean ± s.e.m. of $n=3$ experiments (**f**,**g**,**i**–**k**) or mean ± s.d. of $n=4$ experiments (**h**). Differences relative to DMSO were assessed using a repeated-measures one-way ANOVA; $^{*}P<0.05$, $^{**}P<0.01$, $^{***}P<0.001$ (**f**–**k**). (**l**) Schematic of mTOR inhibition. Western blot was performed using wBM or $CD71^+Ter119^+$ erythroid cells. i.p., intraperitoneal. (**m**) Blood counts in mice treated with Veh ($n=7$), PP242 ($n=5$) or Torin1 ($n=5$). (**n**) Frequencies of BM haematopoietic lineages in mice treated with Veh ($n=6$), PP242 ($n=5$) or Torin1 ($n=5$). (**o**) Erythroid differentiation was assessed by CD71 and Ter119. (**p**) Mitochondrial mass was determined by MitoTracker Green. (**q**) MMP was determined by JC1 staining. Results are mean ± s.e.m. of Veh ($n=4$), PP242 ($n=3$) or Torin1 ($n=3$), and analysed by a two-tailed *t*-test; $^{*}P<0.05$, $^{**}P<0.01$; NS, not significant (**m**–**q**). (**r**) Depletion of TSC1 or TSC2 in erythroid cells increased mtDNA and mitochondrial mass. Results are mean ± s.e.m. of $n=3$ experiments. Differences relative to shNT were assessed using a repeated-measures one-way ANOVA. $^{*}P<0.05$, $^{**}P<0.01$. See Statistics Source Data in Supplementary Table 8. Unprocessed original scans of blots are shown in Supplementary Fig. 9.

mitochondrial mass and impaired erythroid differentiation (Supplementary Fig. 7l,m). Additionally, overexpression of TFAM increased mtDNA and rendered erythroid cells less sensitive to mTORC1 inhibition (Supplementary Fig. 7n–t). Together our results demonstrate that mTORC1 inhibition impaired translation of mitochondria-associated proteins during erythropoiesis.

### Translation of mitochondria-associated proteins is sensitive to mTORC1 inhibition

To investigate whether erythroid mitochondria are selectively sensitive to mTORC1 inhibition, we differentiated HSPCs into erythroid cells and granulocytes (Fig. 8a and Supplementary Fig. 8a–c). By polysome profiling, we observed that PP242 markedly inhibited protein synthesis in erythroid cells, as illustrated by decreased polysome content with a concomitant increase in the 80S peak (Fig. 8b). PP242 did not cause complete disassembly of polysomes, indicating that it selectively impaired a subset of mRNAs[31,32]. Notably, PP242 suppressed the translation of mitochondria-associated mRNAs by shifting these mRNAs towards lighter polysome and monosome fractions (Fig. 8c). In contrast, mTORC1 inhibition in granulocytes had minimal impact on polysome profiles or distribution of mitochondrial mRNAs. Granulocyte differentiation remained ostensibly normal following mTORC1 inhibition or TFAM depletion. Moreover, granulocyte-specific *Tfam* KO by Mrp8-Cre-ires-GFP[33] had minimal effect on $Mac1^{+}Gr1^{+}$ granulocytes or the expression of granulocytic genes (Supplementary Fig. 8d–l), suggesting a distinctive requirement for *Tfam* in erythroid versus granulocyte differentiation.

We next performed iTRAQ-based proteomics of PP242-treated erythroid cells and granulocytes (Fig. 8d). Specifically, 935 proteins were significantly downregulated (fold change $\geq$1.3, $P$ value $\leq$ 0.01) in PP242-treated erythroid cells. Among them, 205 and 245 are Protein-only (Fig. 2a) and mitochondria-associated genes[7,8], which is significantly more enriched than genomic average. In contrast, among 529 downregulated proteins in PP242-treated granulocytes, only 50 and 33 are Protein-only and mitochondrial genes, respectively. Specifically, the expression of mitochondria-associated proteins was downregulated in PP242-treated erythroid cells but not granulocytes (Fig. 8e). Moreover, mitochondria-associated pathways were among the top enriched GO terms in downregulated proteins in erythroid cells but not granulocytes (Fig. 8f). These findings suggest that mitochondria-associated mRNAs are selectively sensitive to enhanced protein translation in erythroid cells.

### Mitochondria-associated mRNAs are regulated by mTORC1

Transcripts regulated by mTORC1 typically have 5′ terminal oligopyrimidine (TOP) or TOP-like motifs[32] consisting of at least five pyrimidines within four nucleotides of transcription start site (TSS). By mapping TSS using dbTSS[34], RefSeq and Ensembl, we found that *TFAM*, *PHB2*, *ATP5A1*, *ATP5B* and *ATP5D* transcripts contain TOP or TOP-like motifs, whereas *ATP5O* contains a translation initiator of short 5′UTR (TISU) motif found in mTOR-sensitive non-TOP mRNAs[35–37] (Fig. 8g). The Protein-only genes were significantly enriched with TOP-like motifs (Fig. 8h).

To test the role of TOP-like motifs, we engineered *TFAM*, *PHB2* and *ATP5D* 5′UTRs containing the wild-type (WT) or mutated (MUT) TOP-like motifs to a GFP reporter and a TK promoter (Fig. 8i and Supplementary Fig. 8m). Following integration into erythroid cells, the MUT sequences decreased GFP expression compared with WT. Notably, PP242 treatment led to significant downregulation of GFP containing WT but not MUT 5′UTRs, suggesting that the TOP-like motifs mediate the modulation of protein translation by mTORC1. In contrast, the expression of GFP remained low and unchanged in granulocytes in the presence or absence of PP242.

Our results support a model that mitochondrial biogenesis is coordinately regulated through mTORC1-mediated protein translation during erythropoiesis (Fig. 8j). Specifically, as erythroid cells differentiate, they acquire erythropoietin (Epo) responsiveness, accumulate iron, and become highly proliferative. Both Epo and iron activate mTORC1 (refs 23,38), which phosphorylates 4EBP1 and S6K to promote synthesis of mitochondrial proteins. Stimulating mitochondrial activity engenders not only intracellular metabolism, but also increased ATP to fuel increasing cellular processes such as haemoglobin synthesis. Thus, our studies identify an essential role for the mTORC1-mitochondria axis in coordinating protein translation and energy metabolism. Mitochondrial dysfunction leads to a variety of human disorders with impaired erythropoiesis being a severe manifestation in a subset of these diseases. Our findings may have direct relevance to the haematologic defects associated with mitochondrial diseases and ageing.

## DISCUSSION

Here we describe the genome-scale comparison of transcriptomic and proteomic changes during human erythropoiesis, and identify mTORC1 as a major modulator of mitochondrial biogenesis. mTORC1 signalling is enhanced through Epo–JAK–AKT signalling[38] or intracellular iron[23] during erythroid differentiation. Elevated mTORC1 increases the translation of mitochondrial mRNAs through the TOP-like motifs, resulting in enhanced mitochondrial activities. mTORC1 also inhibits autophagy, a major pathway in mitochondria degradation[39]. Moreover, mTORC1 promotes mitochondrial function through YY1–PGC1α and HIF1α transcriptional complexes[40,41]. Hence, it is likely that mTORC1 stimulates mitochondrial function by orchestrating translation and transcription of distinct mitochondria-related genes.

Accumulating evidence indicates that deregulated protein translation underlies many blood disorders. Of note, 5q-syndrome and Diamond–Blackfan anaemia (DBA) are caused by ribosomal protein haploinsufficiency[42], and can be ameliorated by L-leucine, which activates mTORC1 signalling[43–45]. Thus, our findings suggest that inhibition of mTOR not only impacts protein translation[45], but also mitochondrial biogenesis resulting in energy imbalance and metabolic dysfunction. Paradoxically, mTORC1 is viewed as a general regulator of protein translation. Thus it is important to determine how and why erythroid cells are specifically sensitive to mTORC1. By comparing two haematopoietic lineages, we provide evidence that mitochondrial protein translation and erythropoiesis are selectively sensitive to mTORC1. First, polysome analysis showed increased translation of mitochondria-associated proteins in erythrocytes but not granulocytes. Second, TFAM depletion or mTORC1 inhibition impaired mitochondria and erythropoiesis, whereas granulocytes were largely spared. Third, acute inhibition of mTORC1 in mice impaired erythropoiesis with minimal impact on other haematopoietic lineages. Finally, while *Tfam* KO was incompatible with erythropoiesis, granulocytes remained ostensibly normal.

Our studies suggest that enhanced mitochondrial biogenesis may be a unique feature of erythropoiesis. Developing erythrocytes are characterized by increasing haem and iron–sulfur cluster biosynthesis in the mitochondria. TFAM-deficient erythroid cells failed to silence HSPC-specific genes, increased histone acetylation and displayed

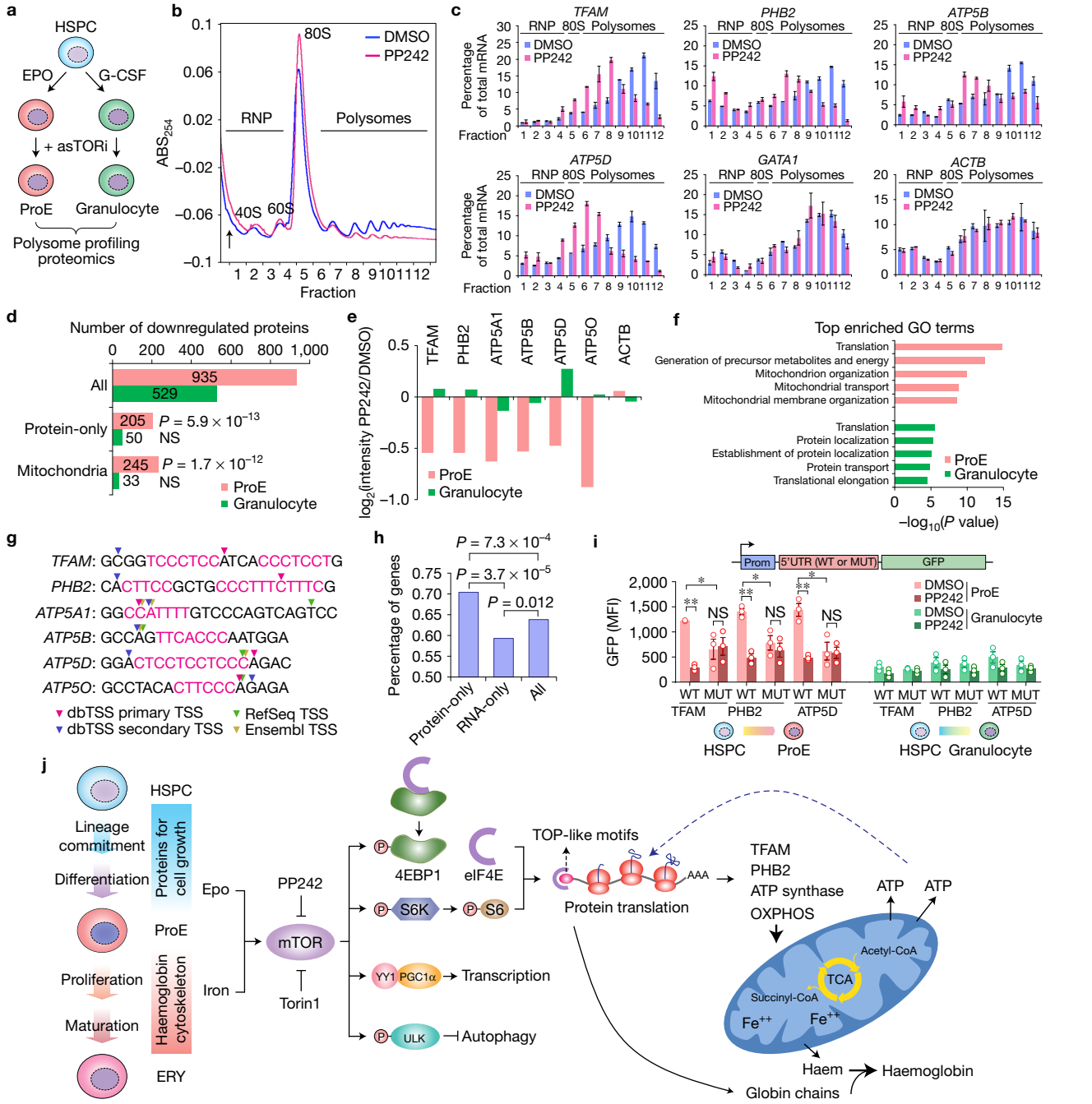


**Figure 8** mTORC1 selectively regulates protein translation of mitochondria-associated mRNAs in erythroid cells. (**a**) Schematic of *ex vivo* differentiation of human primary HSPCs into ProEs or granulocytes. (**b**) A representative profile is shown for polysome profiling of human erythroid cells treated with control (DMSO) or PP242 (2.5 μM) for 12 h. (**c**) qRT–PCR analysis of the indicated transcripts in cells treated with DMSO or PP242. Results are mean ± s.d. of $n = 4$ independent measurements and shown as the percentage (%) of total mRNA of all fractions combined. (**d**) The number of downregulated proteins (fold change ≥ 1.3, $P \leq 0.01$), Protein-only, or mitochondrial proteins were determined by iTRAQ-based proteomics in ProEs or granulocytes treated with PP242 (2.5 μM) or control (DMSO) for 12 h. *P* values were calculated by hypergeometric distribution using All ($n = 935$ and 529 in ProEs and granulocytes, respectively), Protein-only ($n = 205$ and 50) and Mitochondria ($n = 245$ and 33) genes. NS, not significant. (**e**) The changes in the levels of the indicated proteins were determined by iTRAQ-based proteomics in ProEs or granulocytes treated with PP242. Results are shown for one representative proteomic experiment. (**f**) Top enriched GO terms of proteins downregulated in PP242-treated ProEs or granulocytes. (**g**) The most frequent TSS of the indicated transcripts were annotated using dbTSS, RefSeq and Ensembl databases. The sequences of TOP, TOP-like or TISU motifs were shown as the pink colour. (**h**) The frequency of TOP-like motifs in Protein-only, RNA-only or All genes. *P* values were calculated by hypergeometric distribution using All ($n = 4{,}228$ out of 6,624 total detected proteins), Protein-only ($n = 418$ out of 594 total detected proteins) and RNA-only ($n = 363$ out of 612 total detected proteins) genes. (**i**) Mutation of TOP-like motifs at the 5′UTRs of *TFAM*, *PHB2* and *ATP5D* impaired GFP reporter expression in human primary erythroid cells but not granulocytes. Cells treated with control (DMSO) or PP242 (2.5 μM) for 12 h were analysed. Results are mean ± s.e.m. of $n = 3$ independent experiments and analysed by a two-tailed *t*-test. $^{*}P < 0.05$, $^{**}P < 0.01$; NS, not significant. See Statistics Source Data in Supplementary Table 8. (**j**) Model of mTORC1-mediated post-transcriptional control of mitochondrial biogenesis during erythropoiesis.

defective metabolism. Most importantly, the ketone body βOHB, which functions as a potent HDAC inhibitor and is a marker of mitochondrial deficiency in humans, was significantly upregulated. Increased βOHB impaired erythroid differentiation and gene expression similar to TFAM depletion or mTORC1 inhibition. Therefore, our findings provide a molecular link between mitochondrial biogenesis, metabolism and epigenetic regulation indispensable for erythropoiesis. These results are conceptually consistent with the observations of Ansó *et al.* that the mitochondrial respiratory chain is essential for hematopoietic stem cell (HSC) function through regulation of metabolites associated with epigenetic activities[46]. Furthermore, our findings provide a mechanistic explanation for the broader notion that RBCs are uniquely sensitive to deregulated protein translation and/or mitochondria. In light of recent development of inhibitors for protein translation[47], our study raises the possibility that modulation of mitochondrial protein translation may provide therapeutic opportunities for hereditary anaemias and mitochondria-based syndromes. Finally, our results demonstrate how unbiased analysis of proteomic and transcriptomic profiles may identify uncharacterized pathways in cellular regulation. With the increasing availability of genomic and proteomic landscapes, the integrative approach developed here can be extended to the systematic investigation of the gene–protein–pathway networks in health and disease. □

## METHODS

Methods, including statements of data availability and any associated accession codes and references, are available in the online version of this paper.

*Note: Supplementary Information is available in the online version of the paper*

### ACKNOWLEDGEMENTS

We thank S. H. Orkin and L. I. Zon for assistance and discussion, Z. Zhou and Y. Liu for assistance with polysome profiling, U. Eskiocak, S. Yuan, S. Hasan and J. Sudderth at the Children's Research Institute at UT Southwestern, USA for reagents and discussion, and P. Mishra for critical reading of the manuscript. We thank B. van Handel and H. Mikkola at UCLA, USA for providing the fetal $CD34^+$ cells. This work was supported by NIH grants R35CA197532 (to N.S.C.) and T32HL076139 (to S.E.W.), by the Program for Professor of Special Appointment (Eastern Scholar) at Shanghai Institute of Higher Learning (TP2015003) (to F.Z.), by the 100-Talent Program of the Chinese Academy of Sciences (Y516C11851 to Z.S.) and the Science and Technology Commission of Shanghai Municipality (14PJ1410000 to Z.S. and 16ZR1448600 to Y.Z.), by NIH grants K01DK093543, R03DK101665 and R01DK111430, by a Cancer Prevention and Research Institute of Texas (CPRIT) New Investigator award (RR140025), by the American Cancer Society award (IRG-02-196) and the Harold C. Simmons Comprehensive Cancer Center at UT Southwestern, and by an American Society of Hematology Scholar Award (to J.X.).

### AUTHOR CONTRIBUTIONS

J.X. conceived the project. X.L., M.N., H.C., D.L., Z.G. and J.X. performed experiments and analysed the data. F.Z. performed the proteomic profiling and analysed the data. Y.Z., Z.S., M.N., M.L., F.Z. and J.X. performed bioinformatic analyses. R.A.J.S. performed HPG incorporation experiments and analysed the data. Z.H., M.N. and R.J.D. performed the metabolomic profiling and analysed the data. S.E.W. and N.S.C. contributed the *Tfam* flox mouse strain. J.X. wrote the manuscript and X.L., Y.Z., M.N., K.E.D., F.Z. and Z.S. edited it.

### COMPETING FINANCIAL INTERESTS

The authors declare no competing financial interests.

Published online at http://dx.doi.org/10.1038/ncb3527
Reprints and permissions information is available online at www.nature.com/reprints
Publisher's note: Springer Nature remains neutral with regard to jurisdictional claims in published maps and institutional affiliations.

1. Kim, M. S. *et al.* A draft map of the human proteome. *Nature* **509,** 575–581 (2014).
2. Wilhelm, M. *et al.* Mass-spectrometry-based draft of the human proteome. *Nature* **509,** 582–587 (2014).
3. Orkin, S. H. & Zon, L. I. Hematopoiesis: an evolving paradigm for stem cell biology. *Cell* **132,** 631–644 (2008).
4. Rivella, S. Ineffective erythropoiesis and thalassemias. *Curr. Opin. Hematol.* **16,** 187–194 (2009).
5. Xu, J. *et al.* Combinatorial assembly of developmental stage-specific enhancers controls gene expression programs during human erythropoiesis. *Dev. Cell* **23,** 796–811 (2012).
6. Pruitt, K. D. *et al.* RefSeq: an update on mammalian reference sequences. *Nucleic Acids Res.* **42,** D756–D763 (2014).
7. Szklarczyk, D. *et al.* STRING v10: protein–protein interaction networks, integrated over the tree of life. *Nucleic Acids Res.* **43,** D447–D452 (2015).
8. Mootha, V. K. *et al.* Integrated analysis of protein composition, tissue diversity, and gene regulation in mouse mitochondria. *Cell* **115,** 629–640 (2003).
9. Zhang, J., Socolovsky, M., Gross, A. W. & Lodish, H. F. Role of Ras signaling in erythroid differentiation of mouse fetal liver cells: functional analysis by a flow cytometry-based novel culture system. *Blood* **102,** 3938–3946 (2003).
10. Babu, M. M., Luscombe, N. M., Aravind, L., Gerstein, M. & Teichmann, S. A. Structure and evolution of transcriptional regulatory networks. *Curr. Opin. Struct. Biol.* **14,** 283–291 (2004).
11. Vaquerizas, J. M., Kummerfeld, S. K., Teichmann, S. A. & Luscombe, N. M. A census of human transcription factors: function, expression and evolution. *Nat. Rev. Genet.* **10,** 252–263 (2009).
12. Larsson, N. G. *et al.* Mitochondrial transcription factor A is necessary for mtDNA maintenance and embryogenesis in mice. *Nat. Genet.* **18,** 231–236 (1998).
13. Wang, J. *et al.* Dilated cardiomyopathy and atrioventricular conduction blocks induced by heart-specific inactivation of mitochondrial DNA gene expression. *Nat. Genet.* **21,** 133–137 (1999).
14. Signer, R. A., Magee, J. A., Salic, A. & Morrison, S. J. Haematopoietic stem cells require a highly regulated protein synthesis rate. *Nature* **509,** 49–54 (2014).
15. Subramanian, A. *et al.* Gene set enrichment analysis: a knowledge-based approach for interpreting genome-wide expression profiles. *Proc. Natl Acad. Sci. USA* **102,** 15545–15550 (2005).
16. Heinrich, A. C., Pelanda, R. & Klingmuller, U. A mouse model for visualization and conditional mutations in the erythroid lineage. *Blood* **104,** 659–666 (2004).
17. Kaelin, W. G. Jr & McKnight, S. L. Influence of metabolism on epigenetics and disease. *Cell* **153,** 56–69 (2013).
18. Shimazu, T. *et al.* Suppression of oxidative stress by β-hydroxybutyrate, an endogenous histone deacetylase inhibitor. *Science* **339,** 211–214 (2013).
19. Wellen, K. E. *et al.* ATP-citrate lyase links cellular metabolism to histone acetylation. *Science* **324,** 1076–1080 (2009).
20. Larsson, O. *et al.* Distinct perturbation of the translatome by the antidiabetic drug metformin. *Proc. Natl Acad. Sci. USA* **109,** 8977–8982 (2012).
21. Morita, M. *et al.* mTORC1 controls mitochondrial activity and biogenesis through 4E-BP-dependent translational regulation. *Cell Metab.* **18,** 698–711 (2013).
22. Zoncu, R., Efeyan, A. & Sabatini, D. M. mTOR: from growth signal integration to cancer, diabetes and ageing. *Nat. Rev. Mol. Cell Biol.* **12,** 21–35 (2011).
23. Knight, Z. A., Schmidt, S. F., Birsoy, K., Tan, K. & Friedman, J. M. A critical role for mTORC1 in erythropoiesis and anemia. *eLife* **3,** e01913 (2014).
24. Magee, J. A. *et al.* Temporal changes in PTEN and mTORC2 regulation of hematopoietic stem cell self-renewal and leukemia suppression. *Cell Stem Cell* **11,** 415–428 (2012).
25. Roux, P. P. & Topisirovic, I. Regulation of mRNA translation by signaling pathways. *Cold Spring Harb. Perspect. Biol.* **4,** a012252 (2012).
26. Feldman, M. E. *et al.* Active-site inhibitors of mTOR target rapamycin-resistant outputs of mTORC1 and mTORC2. *PLoS Biol.* **7,** e38 (2009).
27. Thoreen, C. C. *et al.* An ATP-competitive mammalian target of rapamycin inhibitor reveals rapamycin-resistant functions of mTORC1. *J. Biol. Chem.* **284,** 8023–8032 (2009).
28. Guo, F. *et al.* Mouse gene targeting reveals an essential role of mTOR in hematopoietic stem cell engraftment and hematopoiesis. *Haematologica* **98,** 1353–1358 (2013).
29. Lamb, R. F. *et al.* The TSC1 tumour suppressor hamartin regulates cell adhesion through ERM proteins and the GTPase Rho. *Nat. Cell Biol.* **2,** 281–287 (2000).
30. Yilmaz, O. H. *et al.* Pten dependence distinguishes haematopoietic stem cells from leukaemia-initiating cells. *Nature* **441,** 475–482 (2006).
31. Hsieh, A. C. *et al.* The translational landscape of mTOR signalling steers cancer initiation and metastasis. *Nature* **485,** 55–61 (2012).
32. Thoreen, C. C. *et al.* A unifying model for mTORC1-mediated regulation of mRNA translation. *Nature* **485,** 109–113 (2012).
33. Passegue, E., Wagner, E. F. & Weissman, I. L. JunB deficiency leads to a myeloproliferative disorder arising from hematopoietic stem cells. *Cell* **119,** 431–443 (2004).
34. Suzuki, A. *et al.* DBTSS as an integrative platform for transcriptome, epigenome and genome sequence variation data. *Nucleic Acids Res.* **43,** D87–D91 (2015).
35. Elfakess, R. *et al.* Unique translation initiation of mRNAs-containing TISU element. *Nucleic Acids Res.* **39,** 7598–7609 (2011).
36. Gandin, V. *et al.* nanoCAGE reveals 5′ UTR features that define specific modes of translation of functionally related MTOR-sensitive mRNAs. *Genome Res.* **26,** 636–648 (2016).
37. Sinvani, H. *et al.* Translational tolerance of mitochondrial genes to metabolic energy stress involves TISU and eIF1-eIF4GI cooperation in start codon selection. *Cell Metab.* **21,** 479–492 (2015).

38. Zhang, X. *et al.* FOXO3-mTOR metabolic cooperation in the regulation of erythroid cell maturation and homeostasis. *Am. J. Hematol.* **89,** 954–963 (2014).
39. Fleming, A., Noda, T., Yoshimori, T. & Rubinsztein, D. C. Chemical modulators of autophagy as biological probes and potential therapeutics. *Nat. Chem. Biol.* **7,** 9–17 (2011).
40. Cunningham, J. T. *et al.* mTOR controls mitochondrial oxidative function through a YY1-PGC-1α transcriptional complex. *Nature* **450,** 736–740 (2007).
41. Duvel, K. *et al.* Activation of a metabolic gene regulatory network downstream of mTOR complex 1. *Mol. Cell* **39,** 171–183 (2010).
42. Narla, A. & Ebert, B. L. Ribosomopathies: human disorders of ribosome dysfunction. *Blood* **115,** 3196–3205 (2010).
43. Jaako, P. *et al.* Dietary L-leucine improves the anemia in a mouse model for Diamond-Blackfan anemia. *Blood* **120,** 2225–2228 (2012).
44. Payne, E. M. *et al.* L-Leucine improves the anemia and developmental defects associated with Diamond-Blackfan anemia and del(5q) MDS by activating the mTOR pathway. *Blood* **120,** 2214–2224 (2012).
45. Chung, J. *et al.* The mTORC1/4E-BP pathway coordinates hemoglobin production with L-leucine availability. *Sci. Signal.* **8,** ra34 (2015).
46. Ansó, E. *et al.* The mitochondrial respiratory chain is essential for haematopoietic stem cell function. *Nat. Cell Biol.* http://dx.doi.org/10.1038/ncb3529 (2017).
47. Skrtic, M. *et al.* Inhibition of mitochondrial translation as a therapeutic strategy for human acute myeloid leukemia. *Cancer Cell* **20,** 674–688 (2011).

DOI: 10.1038/ncb3527

## METHODS

**Cells and cell culture.** Human adult $CD34^+$ HSPCs were obtained from the Fred Hutchinson Cancer Research Center. Fetal liver $CD34^+$ HSPCs were isolated as described previously[48]. ProEs were generated as described previously[5]. Briefly, $CD34^+$ HSPCs were cultured in StemSpan SFEM with 1×CC100 cytokine cocktail (StemCell Technologies) and 2% penicillin–streptomycin for 6 days with medium changes every 2–3 days. On day 6, cells were transferred into StemSpan SFEM with 2% penicillin–streptomycin, Epo (1 U $ml^{-1}$), IL-3 (5 ng $ml^{-1}$), SCF (20 ng $ml^{-1}$), dexamethasone (2 μM) and β-oestradiol (1 μM) with medium changes every 2–3 days. Primary granulocytes were generated from $CD34^+$ HSPCs as described previously[49] with modifications. Briefly, HSPCs were expanded in StemSpan SFEM with 1×CC100 and 2% penicillin–streptomycin for 3 days. Cells were transferred to IMDM with 10% fetal bovine serum (FBS), IL-3 (100 ng $ml^{-1}$) and SCF (100 ng $ml^{-1}$) for 3 days. Cells were then transferred to IMDM with 10% FBS, IL-3 (100 ng $ml^{-1}$), SCF (100 ng $ml^{-1}$) and G-CSF (10 ng $ml^{-1}$), and maintained at 2–8 × $10^5$ cells $ml^{-1}$ with medium changes every 2–3 days. Maturing granulocytes (neutrophils) typically emerge by 7–10 days and can be cultured up to 14 days. For mTORC1 inhibition, cells were treated with control (DMSO), PP242 (2.5 and 10 μM), Torin1 (0.25 and 1 μM) or rapamycin (10 nM, 100 nM and 1 μM) for 5–7 days. No cell lines used in this study were found in the database of commonly misidentified cell lines that is maintained by ICLAC and NCBI BioSample. All cell lines were tested for mycoplasma contamination.

**Mice.** To obtain *Tfam* conditional knockout mice, the $Tfam^{fl/fl}$ mice[12] were crossed with the EpoR-Cre knock-in mice[16] or the Mrp8-Cre-ires-GFP transgenic mice[33]. To obtain *Pten* conditional knockout mice, the $Pten^{fl/fl}$ mice[30] were crossed with the *Mx1-Cre* mice[50]. *Pten* deletion was achieved by intraperitoneal (i.p.) administration of five doses of polyI–polyC (0.8 μg $g^{-1}$ of body weight). PP242 and Torin1 were prepared at 1 mg $ml^{-1}$ and 2 mg $ml^{-1}$ in PBS with 5% PEG400 and 5% Tween80, and administrated via i.p. injection daily at 10 mg $kg^{-1}$ and 20 mg $kg^{-1}$ for 3 days, respectively. All experiments were performed with the approval of the University of Texas Southwestern Institutional Animal Care and Use Committee.

**Quantitative proteomics analysis.** Proteomic analysis was performed as described previously with modifications[51]. We optimized major components of the platform to achieve genome-scale coverage. First, we used high-pH reversed phase (RP) and strong anion exchange (SAX) separation stages coupled with a narrow-bore extended-length low-pH RP column to achieve temporal separation of peptides in a nanoflow regime. Second, we chose the final dimension column geometry to maintain the integrity of chromatopgraphic separation at ultralow effluent flow rates to maximize electrospray ionization efficiency. Third, we implemented separation stages in microcapillary format coupled to the mass spectrometer, thus providing automated and efficient transfer of peptides across all separation stages.

*Sample preparation for DEEP SEQ analysis.* Proteins were extracted with 8 M urea in 0.1 M $NH_4HCO_3$, reduced by 10 mM dithiothreitol (DTT) for 60 min, and alkylated by 20 mM methyl methanethiosulfonate for 30 min. After overnight trypsin digestion at 37 °C, the peptides were cleaned using SepPak C18 RP cartridges (Waters Corp.), labelled with 4-plex iTRAQ reagents (AB Sciex), mixed and loaded into an online chromatography system.

*Multi-dimension separation and data acquisition.* Nanoscale three-dimensional online chromatography consists of a first-dimension RP column (200 μm I.D. capillary packed with 20 cm of 5 μm dia. XBridge C18 resin), a second-dimension SAX column (200 μm I.D. 20 cm of 10 μm dia. POROS10HQ resin) and a third-dimension RP column (25 μm I.D. 120 cm of 5 μm dia. Monitor C18, integrated 1 μm dia. emitter tip). The final dimension ran at ∼5 nl $min^{-1}$ with a 600 min gradient from 2% A to 50% B (A = 0.1% formic acid, B = acetonitrile with 0.1% formic acid). The downstream TripleTOF 5,600+ (AB Sciex) was set in information-dependent mode (IDA). The top 50 precursors (charge state +2 to +5, >100 counts) in each MS scan (800 ms, scan range 350–1,500 $m/z$) were subjected to MS/MS (minimum time 140 ms, scan range 100–1,400 $m/z$). Electrospray voltage was 2.2 kV.

*Data processing and protein identification.* MS data were subjected to a search against the SwissProt database with ProteinPilot V.4.5 (AB Sciex) with the search parameter 'iTRAQ 4-plex (peptides labelling) with 5600 TripleTOF'. The peptide spectra match (PSM) false discovery rate (FDR) ≤ 1% was used to filter peptides. We then summed the intensity of each iTRAQ reporter ion for the peptides assigned to a single gene to generate a ratio for each gene.

*Protein quantification.* To determine the significance of the differences in protein expression, we used a statistical model as described previously[52] with modifications. Specifically, two hypotheses are used: the $\log_2$ ratio of a non-differentially expressed gene's protein counts in two samples follows a normal distribution $N(0,\sigma^2)$, in which 0 is the mean and $\sigma^2$ is the variance that decays exponentially with the gene's average signal intensity[52]; and the majority of genes are non-differentially expressed. In this model, a sliding window of 500 genes moving along the axis of $\log_{10}$ (intensity) was introduced and the distribution of $\log_2$ ratio of genes was considered as a mixture of the normal distribution $N(0,\sigma^2)$ contributed by non-differentially expressed genes and $\log_2$ ratio far from 0 contributed by differentially expressed proteins. To get the $\sigma$, we applied linear regression between the percentiles of the $\log_2$ ratio against the theoretical percentiles of normal distribution $N(0,1)$ from 25% to 75%. The slope was taken as an approximation of the $\sigma$ of the normal distribution followed by the underlying non-differentially expressed proteins. We fitted an exponential decay function $\sigma^2 = \beta \times \exp(\alpha \times \log_{10}(\text{average intensity of window}))$ between the $\sigma^2$ of each window and the average intensity of the proteins. Finally, the $\sigma^2$ of each gene is calculated from the exponential decay function to measure the technical variations and to determine the significance ($P$ value) of its $\log_2$ ratio. A protein was considered to be differentially expressed if the following criteria were met in at least two out of the five replicates: iTRAQ intensity ≥ 300; iTRAQ ratio ≥ 1.3; and $P$ value ≤ 0.01. However, because peptide ratios measured by MS can be distorted during precursor ion isolation[53], the variation in some protein expression may be substantially underestimated. The proteomic experiments were performed as five independent proteome measurements and biological triplicates for the erythroid differentiation experiments. We identified 461,962 distinct peptides (FDR ≤ 1%) from 12,892,243 spectra. After removing genes with weak quantification signal (iTRAQ intensities < 300), we achieved high-quality quantification of proteins encoded by 14,502 genes from 350,843 unique peptide sequences, accounting for 72.4% of annotated RefSeq genes[6].

**Polysome profiling.** Polysome profiling was performed as described previously with modifications[54]. Briefly, cells were treated with 100 μg $ml^{-1}$ cycloheximide (CHX) for 5 min, harvested, washed twice with PBS containing 100 μg $ml^{-1}$ CHX, and centrifuged at 300*g* for 5 min at 4 °C. Cells were resuspended in 425 μl hypotonic buffer (5 mM Tris-HCl pH 7.5, 2.5 mM $MgCl_2$, 1.5 mM KCl, protease inhibitor cocktail) and transferred to a pre-chilled 1.5 ml tube. Then 5 μl of 10 mg $ml^{-1}$ CHX, 1 μl of 1 M dithiothreitol, and 100 U RNase inhibitors were added to cells followed by vortexing for 5 s. Then 25 μl of 10% Triton X-100 and 25 μl of 10% sodium deoxycholate were added to cells followed by vortexing for 5 s. The supernatant were transferred to a pre-chilled 1.5 ml tube after centrifugation at 21,000*g* for 5 min at 4 °C. Aliquots of the same OD amount of lysates from each sample were loaded onto a 10–50% sucrose gradient, and centrifuged at 35,000 r.p.m. for 2 h at 4 °C using a SW40Ti rotor in a Beckman Coulter Optima L-80 ultracentrifuge with no brake. Samples were analysed on the Bio-Rad BioLogic LP system and BioFrac fraction collector, and chased with 60% (w/v) sucrose with bromophenol blue at 1 ml $min^{-1}$. Data were analysed using the Bio-Rad LP Data View software. Polysome fractions were collected at 0.5 ml per fraction. For mTORC1 inhibition, cells were treated with DMSO or 2.5 μM PP242 for 12 h.

**Measurement of protein synthesis.** Protein synthesis was measured by the incorporation of L-homopropargylglycine (HPG)[14]. A total of 0.5–1 × $10^5$ $CD34^+$ HSPCs or ProEs were plated in 100 μl of methionine-free DMEM with 200 μM L-cysteine, 50 μM 2-mercaptoethanol, 1 mM L-glutamine, 0.1% BSA (Sigma) and appropriate cytokines. Cells were pre-cultured for 45 min to deplete endogenous methionine, followed by 1 h incubation with 1 mM HPG. Cells were washed twice with PBS and fixed 15 min in 0.5 ml of 1% paraformaldehyde in PBS on ice, followed by PBS wash and permeabilization in 200 μl PBS containing 3% FBS and 0.1% saponin for 5 min at room temperature. The Click-iT Cell Reaction Buffer Kit (Life Technologies) was used to conjugate azide to Alexa Fluor 488 or Alexa Fluor 555. After 30 min, cells were washed twice in PBS containing 3% FBS and 0.1% saponin, resuspended in PBS containing 4 μg $ml^{-1}$ of 4′,6-diamidino-2-phenylindole (DAPI), and analysed by flow cytometry.

**qRT–PCR and RNA-seq analysis.** RNA was isolated using RNeasy Plus Mini Kit (Qiagen). qRT–PCR was performed using the iQ SYBR Green Supermix (Bio-Rad). RNA-seq library was prepared using the Truseq RNA Library Prep Kit (Illumina). For RNA-seq in HSPCs and ProEs, the raw reads were aligned to human genome (hg19) by TopHat[55]. Differentially expressed genes were identified by DEseq[56] using fold change ≥1.5 and $P$ value ≤ 0.01. For RNA-seq in fetal liver $CD71^+Ter119^+$ erythroid cells, the reads were aligned to mouse genome (mm9) by TopHat[55]. Differentially expressed genes were identified by Cufflinks[57] using fold change ≥1.5 and $P$ value ≤ 0.05.

**Western blot.** Western blot was performed as described previously[5] using the following antibodies: TFAM (7495S, Cell Signaling Technology; sc-23588, Santa Cruz Technology), PHB2 (14085S, Cell Signaling Technology), ATP5A1 (sc-136178, Santa Cruz Technology), ATP5B (sc-16690, Santa Cruz Technology), ATP5D (ab97491, Abcam), ATP5O (ab110276, Abcam, clone 4C11C10D12),

4EBP1 (9644S, Cell Signaling Technology), phos-4EBP1 (Thr37/46) (2855S, Cell Signaling Technology), p70S6K (2708S, Cell Signaling Technology), phos-S6K (Ser235/236) (2211S, Cell Signaling Technology), GATA1 (ab47490, Abcam), GATA2 (ab22849, Abcam), TSC1 (6935, Cell Signaling Technology), TSC2 (4308, Cell Signaling Technology), H3K9ac (9649, Cell Signaling Technology), H3K27ac (8173, Cell Signaling Technology), H3K56ac (4243, Cell Signaling Technology), H4K5ac (ab51997, Abcam), H3K4me3 (9571, Cell Signaling Technology), H3K9me3 (13969, Cell Signaling Technology), H3K27me3 (9733, Cell Signaling Technology), H3K36me3 (4909, Cell Signaling Technology), H3 (4499, Cell Signaling Technology), ACTB (MAB1501, Millipore, clone C4) and GAPDH (sc-26778, Santa Cruz Biotechnology). Densitometry quantification was performed using ImageJ software. All antibodies were used at 1:1,000 dilutions except phos-4EBP1 (1:500), phos-S6K (1:500) and ACTB (1:2,500).

**ChIP-seq analysis.** ChIP-seq was performed as described previously[5,58] using H3K27ac antibody (ab4729, Abcam) in K562 cells. ChIP-seq libraries were generated using NEBNext ChIP-seq Library Prep Master Mix (NEB). ChIP-seq raw reads were aligned to human genome (hg19) using Bowtie[59], and peaks were identified using MACS[60]. Differentially enriched ChIP-seq peaks were identified using MAnorm[58,61]. MAnorm takes the chromosomal coordinates of all peaks and aligned reads in both samples as input. The $(M,A)$ value of each peak was calculated and plotted, where $M = \log_2$ (read density in shTFAM/read density in shNT) and $A = 0.5 \times \log_2$ (read density in shTFAM × read density in shNT). Robust regression was applied to the $(M,A)$ values of common peaks and a linear model was derived. The linear model was extrapolated to all peaks for normalization. The normalized $M$ values represent $\log_2$-transformed fold changes of intensities at each peak between two samples. To identify upregulated or downregulated H3K27ac ChIP-seq peaks, we filtered the differentially enriched peaks on the basis of $M$ values (referred to as $M_{H3K27ac}$). For significantly upregulated or downregulated peaks, we kept H3K27ac peaks with $|M_{H3K27ac}| > 2$; for shared H3K27ac peaks, we used $|M_{H3K27ac}| \leq 2$.

**Mitochondrial DNA, mass and membrane potential.** Mitochondrial DNA (mtDNA) was determined using qPCR to measure the ratio of mtDNA versus genomic DNA. The primer sequences are in Supplementary Table 7. Mitochondrial mass was determined using flow cytometry. Briefly, $0.5–1 \times 10^6$ cells were incubated with 100 nM MitoTracker Green (Invitrogen) and antibodies for cell surface markers for 30 min at 37 °C, and analysed on FACSCanto with 488 nm excitation. Mitochondrial membrane potential (MMP) was monitored by JC1 staining. Briefly, $0.5–1 \times 10^5$ cells were washed with PBS and resuspended in PBS containing 2 μM JC1 and incubated at 37 °C in 5% $CO_2$ for 15 min. The control cells were incubated with 2 μM JC1 with 10 μM protonophore FCCP (carbonyl cyanide 4-(trifluoromethoxy) phenylhydrazone) for 15 min. Cells were washed, resuspended and analysed on FACSCanto.

**Intracellular ATP.** Intracellular ATP was determined using the CellTiter-Glo Luminescent Cell Viability Assay (Promega) following the manufacturer's protocol.

**Metabolite profiling.** Cells ($3–5 \times 10^6$) were harvested, washed twice with ice-cold saline, overlaid with 500 μl of cold methanol/water (50/50, $v/v$), and subjected to three freeze–thaw cycles. After vortexing, the debris was pelleted by centrifugation at 16,000*g* and 4 °C for 15 min and used for protein quantitation. The supernatant was dried using a SpeedVac concentrator, reconstituted in 100 μl of 0.03% formic acid, vortex-mixed and centrifuged to remove debris. Targeted metabolite profiling of ~200 water-soluble endogenous metabolites was performed using an LC–MS/MS approach. Separation was achieved on a Phenomenex Synergi Polar-RP HPLC column (150 × 2 mm, 4 μm, 80 Å) using a Nexera UHPLC system (Shimadzu Corporation). The mobile phases were 0.03% formic acid in water (A) and 0.03% formic acid in acetonitrile (B). The gradient programme was as follows: 0–3 min, 100% A; 3–15 min, 100%–0% A; 15–21 min, 0% A; 21–21.1 min, 0–100% A; 21.1–30 min, 100% A. The column was maintained at 35 °C. Samples were kept in the autosampler at 4 °C with 0.5 ml $min^{-1}$ flow rate and 10 μl injection volume. The mass spectrometer AB QTRAP 5500 (AB SCIEX) was set in multiple-reaction monitoring (MRM) mode. Sample analysis was performed in positive/negative switching mode. Declustering potential (DP) and collision energy (CE) were optimized for each metabolite by direct infusion of reference standards. The MRM MS/MS detector conditions were set as follows: curtain gas 30 psi; ion spray voltages 1,200 V (positive) and −1,500 V (negative); temperature 650 °C; ion source gas 150 psi; ion source gas 250 psi; interface heater on; entrance potential 10 V. The MRM transition ($m/z$) and CE (V) of each metabolite were optimized using standard compound. Dwell time for each transition was 3 ms. MRM data were acquired using Analyst 1.6.1 software (AB SCIEX). Chromatogram review and peak area integration were performed using MultiQuant software version 2.1 (AB SCIEX). The peak area for each metabolite was normalized against the total ion current of all metabolites. The normalized area values were used as variables for the multivariate and univariate statistical analysis. All multivariate analyses were performed using SIMCA-P (version 13.0.1, Umetrics). The pre-processed data sets were mean-centred and unit-variance scaled, and evaluated by principal component analysis. Univariate statistical differences were analysed using a Student's $t$-test.

**Acetyl-CoA and HDAC assays.** Acetyl-CoA was measured using the PicoProbe Acetyl-CoA fluorometric assay kit (BioVision K317-100). HDAC activity was measured using the HDAC activity colorimetric assay kit (BioVision K331-100). Specifically, 1.5 million cells were lysed and diluted to 85 μl in double-distilled $H_2O$ in a 96-well plate. Ten microlitres of 10× HDAC assay buffer and 5 μl of the HDAC colorimetric substrate were added and mixed thoroughly. The plate was incubated at 37 °C for 2 h before adding 10 μl of lysine developer. The plate was incubated at 37 °C for 30 min and measured at 405 nm. HDAC activity was expressed as the relative OD value per milligram of protein.

**Lentiviral RNAi.** Lentiviral RNAi was performed as described previously[5]. The shRNAs in the pLKO.1-puro vector for TFAM (sh1: TRCN0000016095; sh2: TRCN0000016093) and PHB2 (sh1: TRCN0000060920; sh2: TRCN0000060921) were obtained from Sigma-Aldrich. The shRNAs in the pGIPZ vector for TSC1 (sh1: V2LHS_92624) and TSC2 (sh1: V2LHS_233694; sh2: V2LHS_93624) were obtained from GE Dharmacon. Sequences of shRNAs are in Supplementary Table 7.

**Flow cytometry.** Cells were analysed using FACSCanto (BD Biosciences) for expression of CD34, CD71, CD235a or Ter119 conjugated to phycoerythrin (PE), fluorescein isothiocyanate (FITC) or allophycocyanin (APC; BD Pharmingen). Live cells were identified by exclusion of 7-amino-actinomycin D (7-AAD). Haematopoietic lineages in mouse BM were identified using markers for granulocytes ($Gr1^+Mac1^+$), macrophages ($Mac1^+F4/80^+$), immature ($IgM^-B220^+$) and mature B lymphocytes ($IgM^+B220^+$), immature ($CD71^+Ter119^+$) and mature erythroid cells ($CD71^-Ter119^+$). Data were analysed using FlowJo software (Ashland).

**Cytospin and haematological indices.** Cytocentrifuge preparations were stained with May-Grunwald–Giemsa as described previously[62]. Peripheral blood was isolated via the retro-orbital plexus and analysed on a HEMAVET HV950 (Drew Scientific) as described previously[62].

**Statistics and reproducibility.** Data are represented as mean ± standard error of the mean (s.e.m.) or standard deviation (s.d.) of at least three independent experiments as specified in the figure legends. Graphs and statistical analysis were performed using the Microsoft Excel or GraphPad Prism software. Comparisons between groups were performed using the two-sided Student's $t$-test, repeated-measures one-way ANOVA with Dunnett's correction, Fisher exact $t$-test with Benjamini procedure, or hypergeometric distribution, as denoted in figure legends. The numbers of independent experiments or biological replicate samples and $P$ values (NS, not significant; $^*P < 0.05$, $^{**}P < 0.01$, $^{***}P < 0.001$) are provided in individual figures. $P < 0.05$ was considered statistically significant. Panels in Figs 2f, 4c,e,g, 5a,b,d, 6a,j, 7d,e,l and 8d,e and Supplementary Figs 3a,c,f,h, 4b, 5a,c,e, 6b, 7d,g,n and 8a,h show a representative image or flow cytometry of at least three independent experiments or biological replicate samples. Analysis of gene expression was determined using the $2^{-\Delta\Delta Ct}$ method with *GAPDH* as the reference gene unless otherwise specified. No statistical method was used to predetermine sample size in animal studies and the experiments were not randomized. The investigators were not blinded to allocation during experiments and outcome assessment.

**Code availability.** Computation codes are available from the corresponding author on request.

**Data availability.** The RNA-seq data sets for human HSPCs (A0 and F0), ProEs (A5, F5, shNT, shTFAM and shPHB2), E13.5 fetal liver $CD71^+Ter119^+$ erythroid cells (*Tfam* WT and KO), and H3K27ac ChIP-seq data sets have been deposited in the Gene Expression Omnibus (GEO) under the accession number GSE86912. Mass spectrometry data have been deposited in ProteomeXchange with the primary accession code PXD006170. Source data for RNA-seq analysis are provided as Supplementary Tables 2 and 4–6. Source data for proteomic analysis are provided as Supplementary Tables 1, 3 and 4. Statistics source data for Figs 2e,g, 3b–g, 4b,d,f,h–n, 5c,e–h, 6g–l, 7a,c,f–k,m–r and 8c,i and Supplementary Figs 3b,d,e,g,i,j, 4c, 6a,c,d,f, 7a–c,e,f,h–m,o–t and 8c,e–g,i–l are provided in Supplementary Table 8. All other data supporting the findings of this study are available from the corresponding author on request.

48. Van Handel, B. *et al.* The first trimester human placenta is a site for terminal maturation of primitive erythroid cells. *Blood* **116,** 3321–3330 (2010).
49. Gupta, D., Shah, H. P., Malu, K., Berliner, N. & Gaines, P. in *Current Protocols in Immunology* 104 (eds John, E. C. *et al.*) Unit 22F.25 (John Wiley, 2014).

DOI: 10.1038/ncb3527


50. Kuhn, R., Schwenk, F., Aguet, M. & Rajewsky, K. Inducible gene targeting in mice. *Science* **269,** 1427–1429 (1995).
51. Zhou, F. *et al.* Genome-scale proteome quantification by DEEP SEQ mass spectrometry. *Nat. Commun.* **4,** 2171 (2013).
52. Zhang, Y. *et al.* A robust error model for iTRAQ quantification reveals divergent signaling between oncogenic FLT3 mutants in acute myeloid leukemia. *Mol. Cell. Proteomics* **9,** 780–790 (2010).
53. Karp, N. A. *et al.* Addressing accuracy and precision issues in iTRAQ quantitation. *Mol. Cell. Proteomics* **9,** 1885–1897 (2010).
54. Dowling, R. J. *et al.* mTORC1-mediated cell proliferation, but not cell growth, controlled by the 4E-BPs. *Science* **328,** 1172–1176 (2010).
55. Trapnell, C., Pachter, L. & Salzberg, S. L. TopHat: discovering splice junctions with RNA-Seq. *Bioinformatics* **25,** 1105–1111 (2009).
56. Anders, S. & Huber, W. Differential expression analysis for sequence count data. *Genome Biol.* **11,** R106 (2010).
57. Trapnell, C. *et al.* Differential analysis of gene regulation at transcript resolution with RNA-seq. *Nat. Biotechnol.* **31,** 46–53 (2013).
58. Huang, J. *et al.* Dynamic control of enhancer repertoires drives lineage and stage-specific transcription during hematopoiesis. *Dev. Cell* **36,** 9–23 (2016).
59. Langmead, B., Trapnell, C., Pop, M. & Salzberg, S. L. Ultrafast and memory-efficient alignment of short DNA sequences to the human genome. *Genome Biol.* **10,** R25 (2009).
60. Zhang, Y. *et al.* Model-based analysis of ChIP-Seq (MACS). *Genome Biol.* **9,** R137 (2008).
61. Shao, Z., Zhang, Y., Yuan, G. C., Orkin, S. H. & Waxman, D. J. MAnorm: a robust model for quantitative comparison of ChIP-Seq data sets. *Genome Biol.* **13,** R16 (2012).
62. Xu, J. *et al.* Correction of sickle cell disease in adult mice by interference with fetal hemoglobin silencing. *Science* **334,** 993–996 (2011).